การศึกษาเชิงทฤษฎีของรอยต่อ โลหะ-ฉนวน-ตัวนำยวดยิ่ง : ผลของความหนาของชั้นฉนวน

นายรามย์ พิณเจริญพันธุ์

วิทยานิพนธ์นี้เป็นส่วนหนึ่งของการศึกษาตามหลักสูตรปริญญาวิทยาศาสตรมหาบัณฑิต
สาขาวิชาฟิสิกส์
มหาวิทยาลัยเทคโนโลยีสุรนารี
ปีการศึกษา 2549

THEORETICAL STUDY OF METAL-INSULATOR-SUPERCONDUCTOR JUNCTION: EFFECTS OF FINITE INSULATING LAYER THICKNESS

Rarm Phinjaroenphan

A Thesis Submitted in Partial Fulfillment of the Requirements for the Degree of Master of Science in Physics

Suranaree University of Technology

Academic Year 2006

THEORETICAL STUDY OF METAL-INSULATOR-SUPERCONDUCTOR JUNCTION: EFFECTS OF FINITE INSULATING LAYER THICKNESS

Suranaree University of Technology has approved this thesis submitted in partial fulfillment of the requirements for a Master's Degree.

Thesis Examining Committee

_____
(Assoc. Prof. Dr. Prapan Manyum)
Chairperson

_____
(Asst. Prof. Dr. Puangratana Pairor)
Member (Thesis Advisor)

_____
(Prof. Dr. Sukit Limpijumnong)
Member

_____
(Dr. Saroj Rujirawat)
Member

_____ _____
(Assoc. Prof. Dr. Saowanee Rattanaphani) (Assoc. Prof. Dr. Sompong Thammathaworn)
Vice Rector for Academic Affairs Dean of Institute of Science

รามย์ พิณเจริญพันธุ์ : การศึกษาเชิงทฤษฎีของรอยต่อ โลหะ-ฉนวน-ตัวนำยวดยิ่ง: ผลของความหนาของชั้นฉนวน (THEORETICAL STUDY OF METAL-INSULATOR-SUPERCONDUCTOR JUNCTION : EFFECTS OF FINITE INSULATING LAYER THICKNESS) : อาจารย์ที่ปรึกษา : ผู้ช่วยศาสตราจารย์ ดร.พวงรัตน์ ไพเราะ, 58 หน้า.

ในวิทยานิพนธ์นี้ สเปกตรัมของค่าความหนาแน่นกระแส และสภาพการนำไฟฟ้า ของรอยต่อหนึ่งมิติ สองชนิดคือ โลหะ-ฉนวน-โลหะ และ โลหะ-ฉนวน-ตัวนำยวดยิ่ง ได้ถูกศึกษาโดยใช้แบบจำลองที่แตกต่างกันสองชนิด คือ แบบจำลองฟังก์ชันเดลตา และแบบจำลองความหนาจำกัด วิธีการการกระเจิงถูกนำมาใช้ในการคำนวณหาค่าความน่าจะเป็นของการสะท้อนกลับและการส่งผ่าน ซึ่งค่าความน่าจะเป็นดังกล่าวจะถูกนำไปคำนวณหาค่าความหนาแน่นกระแสและสภาพการนำไฟฟ้าที่เป็นฟังก์ชันของความต่างศักย์ที่อุณหภูมิศูนย์องศาสัมบูรณ์

เมื่อค่าความต่างศักย์มีค่าต่ำกว่าค่าความต่างศักย์กีดขวาง แบบจำลองความหนาจำกัดจะให้ผลลัพธ์ใกล้เคียงกับในแบบจำลองฟังก์ชันเดลตาในรอยต่อทั้งสองชนิด เมื่อค่าความต่างศักย์มีค่าสูงกว่าค่าความต่างศักย์กีดขวาง ค่าความหนาแน่นกระแสและสภาพการนำไฟฟ้าในรอยต่อทั้งสองแบบจะมีการแกว่งกวัดขึ้น ซึ่งขึ้นอยู่กับค่าความหนาของชั้นฉนวน ลักษณะการแกว่งกวัดนี้ไม่สามารถอธิบายได้ด้วยแบบจำลองฟังก์ชันเดลตา จากแบบจำลองความหนาจำกัดระยะห่างของจุดยอดถึงจุดยอดลำดับถัดไปมีค่าสอดคล้องกับ $\Delta E_n = \frac{\mathrm{h}^2}{2m}\left(\frac{\pi}{L}\right)^2 (2n+1)$ เมื่อ n คือ เลขจำนวนเต็มบวก

ในวิทยานิพนธ์นี้ยังแสดงให้เห็นอีกว่า แบบจำลองฟังก์ชันเดลตาให้ผลตรงกับแบบจำลองความหนาจำกัดได้ภายใน 10% เมื่อค่าความต่างศักย์มีค่าต่ำกว่าค่าความต่างศักย์กีดขวาง และค่าความหนาของชั้นฉนวนมีค่าเป็น $Lk_F \le \sqrt{\frac{2E_F^{3/2}}{3\sqrt{U}\,(U+E_F)}}$ โดยที่ k_F และ E_F คือ เวคเตอร์คลื่นเฟร์มีและค่าพลังงานเฟร์มี ตามลำดับ ค่าความสัมพันธ์ของตัวแปรเสริมที่บ่งบอกสมบัติของชั้นฉนวนจากแบบจำลองทั้งสอง คือ $Z = \frac{(U+E_F)}{2E_F} Lk_F$ เมื่อ Z คือ ตัวแปรเสริมไม่มีหน่วยที่ใช้บ่งบอกสมบัติของชั้นของฉนวนในแบบจำลองฟังก์ชันเดลตา โดยค่าเงื่อนไขของค่าความหนาและค่าความสัมพันธ์ของตัวแปรเสริมจะมีค่าไม่ขึ้นอยู่กับชนิดของรอยต่อ

สาขาวิชาฟิสิกส์ ลายมือชื่อนักศึกษา_____

ปีการศึกษา 2549 ลายมือชื่ออาจารย์ที่ปรึกษา_____

RARM PHINJAROENPHAN : THEORETICAL STUDY OF METAL-INSULATOR-SUPERCONDUCTOR JUNCTION : EFFECTS OF FINITE INSULATING LAYER THICKNESS. THESIS ADVISOR : ASST. PROF. PUANGRATANA PAIROR, Ph.D. 58 PP.

TUNNELING SPECTROSCOPY/METAL-INSULATOR-SUPERCONDUCTOR JUNCTION/SCATTERING METHOD/INSULATING BARRIER

In this thesis, the current density and conductance spectra of one-dimensional metal-insulator-metal and metal-insulator-superconductor junctions are studied using two different models: Delta-function and Finite-width models. The scattering method is used to calculate reflection and transmission probabilities, which then are used to obtain the current density and conductance at zero temperature as a function of applied voltage.

When the applied voltage is lower than the barrier potential *U*, the Finite-width model produces similar results to the Delta-function model for both types of junctions. When the applied voltage is higher than the barrier potential, both current density and conductance spectra of both types of junctions contain oscillations, which are dependent on the thickness *L* of the insulator. These oscillations cannot be produced in the Delta-function model. Accordingly to the Finite-width model, the distance in energy between two adjacent peaks satisfies $\Delta E_n = \frac{\mathrm{h}^2}{2m}\left(\frac{\pi}{L}\right)^2 (2n+1)$, where n is a positive integer.

It is also shown in this thesis that one can use the Delta-function model in place of the Finite-width model, within 10% accuracy, when the applied voltage is

lower than the barrier potential and when the thickness of the insulating layer satisfies the inequality $Lk_F \leq \sqrt{\frac{2E_F^{3/2}}{3\sqrt{U}(U+E_F)}}$, where k_F and E_F are the Fermi wave vector and energy of the superconductor respectively. The relation among the parameters characterizing the insulator from both models is $Z = \frac{(U+E_F)}{2E_F} Lk_F$, where Z is the unitless parameter describing the insulator is the Delta-function model. Both inequality condition and the relation among the insulating parameters are independent of the types of the junctions.

School of Physics Student's Signature _____

Academic Year 2006 Advisor's Signature _____

ACKNOWLEDGEMENTS

I would like to thank many people for their support and guidance during the development of this thesis work. First of all, I would like to express my sincere gratitude to Asst. Prof. Dr. Puangratana Pairor, my thesis advisor, for her invaluable guidance on all problems throughout this work.

I would also like to thank Assoc. Prof. Dr. Prapan Manyum, Dr. Saroj Rujirawat and Prof. Dr. Sukit Limpijumnong for being on my thesis committee.

I would like to thank all physics graduate students at Suranaree University of Technology for their friendly and sincerely.

Finally, I would like to thank my parents for their support and encouragement over all the years of my life.

Rarm Phinjaroenphan

CONTENTS

Page

CONTENTS (Continued)

Page

LIST OF FIGURES

LIST OF FIGURES (Continued)

Figure **Page**

LIST OF FIGURES (Continued)

Figure **Page**

LIST OF FIGURES (Continued)

Figure **Page**

CHAPTER I

INTRODUCTION

1.1 Motivation

Metal-insulator-superconductor (MIS) tunneling spectroscopy has long been used to study the properties of a superconductor (Wolf, 1989). Because the energy scale involved in the spectroscopy is small, compared to the Fermi energy of the metal, the features in the tunneling conductance spectrum reflect mostly the characteristics of the superconductor (Wolf, 1989). For instance, in the tunneling limit or low transmission limit where the insulating barrier is high, the conductance spectrum of a conventional superconductor is proportional to the density of states of the superconductor (Bardeen, Cooper, and Schrieffer, 1957; Giaever, 1960; Nicol, Shapiro, and Smith, 1960). The energy position where the coherence peak occurs in the spectrum provides an accurate measurement of the magnitude of the superconducting gap (Giaever, 1960; Nicol, Shapiro, and Smith, 1960). In the limit where the barrier is low or in the high transmission limit, the conductance shows the consequence of Andreev reflection (Blonder, Tinkham, and Klapwijk, 1982), the process in which the transfer of two electrons across the interface occurs (Andreev, 1964).

In addition to the physical properties of the superconductor, the geometry of the junction can also affect the features in the conductance spectrum. For instance, the conductance spectrum of a MIS junction may contain oscillations due to the finite

thickness of the superconductor and the metal. The oscillations due to the finite width of the superconductor are called Tomasch oscillations (Tomasch, 1965; Tomasch, 1966) and those due to the finite width of the metal are called Mcmillan-Rowell oscillations (Rowell and McMillan, 1966). The periods of both oscillations depend on the width of the layer, the corresponding Fermi velocity, and the magnitude of the superconducting gap (Rowell and McMillan, 1966; McMillan and Anderson, 1966). These features thus provide a means to measure the Fermi velocity and the magnitude of the superconducting gap (Lykken, Geiger, and Mitchell, 1970; Lykken, Geiger, Dy, and Mitchell, 1971; Tsokur, Yarygin, Yusupov, Aminov, Hein, Muller, Piel, Wehler, Kresin, Rosner, Winzer, and Wolf, 1995; Nesher and Koren, 1999; Nesher and Koren, 1999; Shkedy, Aronov, Koren, and Polturak, 2004). It is clear that there is a lot of physical information that can be extracted from the tunneling data. In order to obtain reliable interpretation, one needs to understand quantitatively how characteristics of the materials making up the junction as well as the junction geometry affect the tunneling conductance spectrum.

The geometry of the insulator can effect to MIS tunneling spectrum as well. As mentioned earlier, when the insulating barrier is high, the conductance spectrum has the same shape as the density of states of the superconductor, whereas when the insulating barrier is low, the conductance spectrum shows the inverted-gap structure due to the Andreev reflection process. It is interesting to study in more details of how the characteristics, not only the potential but also the thickness, of the insulating barrier affect the tunneling spectroscopy of MIS junction.

1.1 Methods of Study

There are at least two theoretical methods widely used to study tunneling junctions: transfer Hamiltonian and scattering method. In the former approach, one assumes that the system is divided into two nearly independent parts by the insulating layer and these parts are coupled by a perturbing Hamiltonian, which requires some microscopic knowledge of the system. With this transfer Hamiltonian one can then determine the tunneling transfer matrix element. The electron transition rate from one side to the other and hence the current can be obtained by using the Fermi Golden Rule (Wolf, 1989). Because this approach is based on the perturbation theory, it is limited to study of those junctions with either high insulating barriers or thick insulating layers.

In order to study the effect of arbitrary thickness and potential barrier strength, a phenomenological scattering method can instead be used. In this formalism (Griffin and Demers, 1971; Blonder, Tinkham, and Klapwijk, 1982), it is assumed that the bulk wave functions of all regions of the junction can be written as a simple linear combination of appropriate wave functions. With suitable matching conditions, which depends on the details of each model, one can obtain the reflection and transmission probabilities and hence the current across the junction. In the high barrier and clean limit with the isotropic superconducting gap, the resulting current from this formalism is equivalent to that from the transfer Hamiltonian method (Blonder, Tinkham, and Klapwijk, 1982).

In this thesis, the scattering method is chosen for the study of MIS junction, for comparison and study the effect of the thickness of the layer. Also, two models are used to represent the insulating layer.

In the first model called Delta-function model, a delta-function potential with height H (in units of energy per length) is used to represent the insulator (Blonder, Tinkham, and Klapwijk, 1982). In this model, it is obvious that the effect of the finite width of the insulating barrier is completely ignored.

In the second model called Finite-width model, the insulator is represented by a more realistic layer of finite thickness (Griffin and Demers, 1971). In this model the calculation is more complicated but more complete.

In this thesis, the theoretical investigation of the dependence on the insulating layer of MIS tunneling spectroscopy is carried out. In order to gain better understanding of the effect of the insulator on MIS tunneling spectroscopy, metal-insulator-metal (MIM) tunneling spectroscopy is also studied as a preamble and for comparison with MIS tunneling spectroscopy.

1.2 Models and Assumptions

Tunneling spectra of two types of junctions, MIM and MIS, are studied using the scattering method in this thesis. The insulating layer of each junction is represented by two different models as defined in the previous section, i.e., Delta-function and Finite-width models. Also, all the junctions are modeled by one-dimensional infinite systems, in which either two semi-infinite metals, or a semi-infinite metal and a semi-infinite superconductor, are joined by either a delta-function like insulating layer, or an insulating layer of arbitrary thickness L, as shown pictorially in Fig. 1.1.

A parabolic energy dispersion relation is used to describe the conduction bands of both metal and insulator, as shown in Fig. 1.2. The Fermi level is set to be in the

metal conduction band and to be *U* below the bottom of the empty conduction band of the insulator.

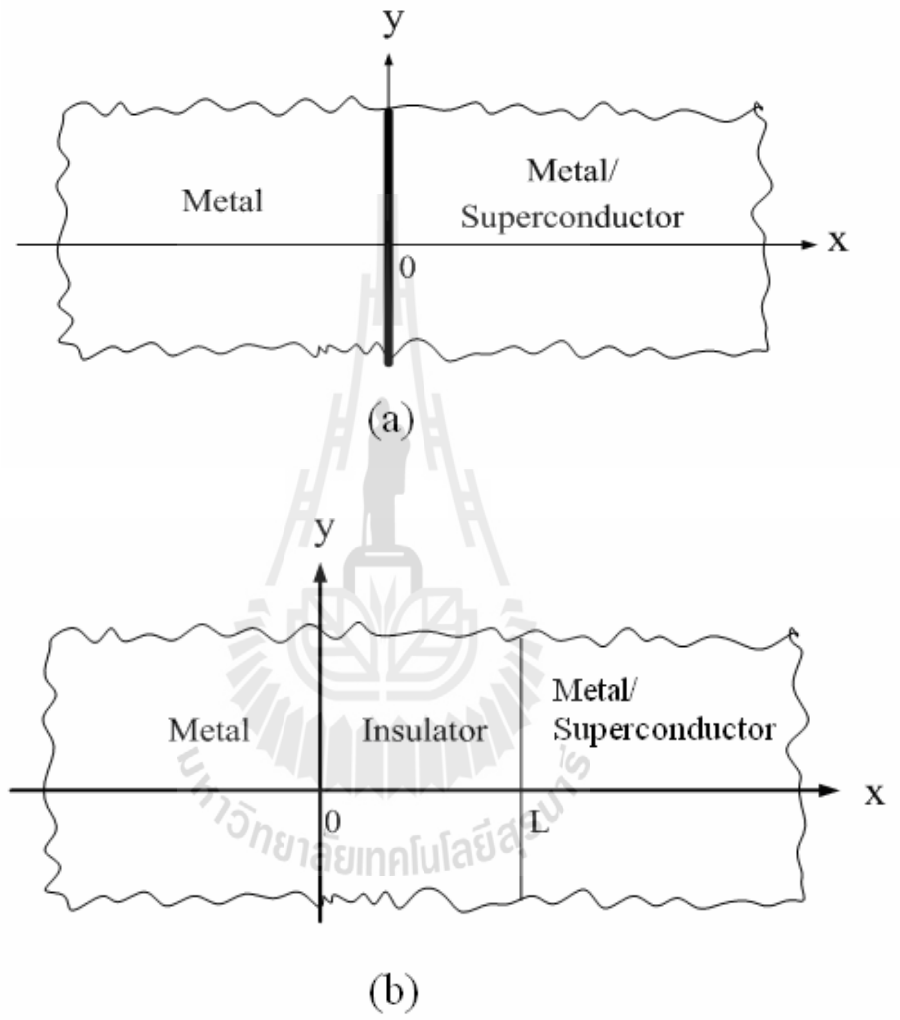

Figure 1.1 Diagram of each type of junction studied in this thesis. Figure (a) shows the Delta-function model and Figure (b) represents the Finite-width model.

For the superconductor, the excitation energy is taken to be

$$E = \sqrt{\left(\frac{\hbar^2 k^2}{2m} - E_F\right)^2 + \Delta^2} \qquad (1.1)$$

where $\vec{k}$ is the Fermi wave vector, m is the mass of a quasiparticle, E_F is Fermi energy and Δ is the superconducting gap, which is taken to be constant and independent of the position in the superconducting region. Both the suppression of the superconducting gap near the surface and the proximity effect are ignored in this thesis.

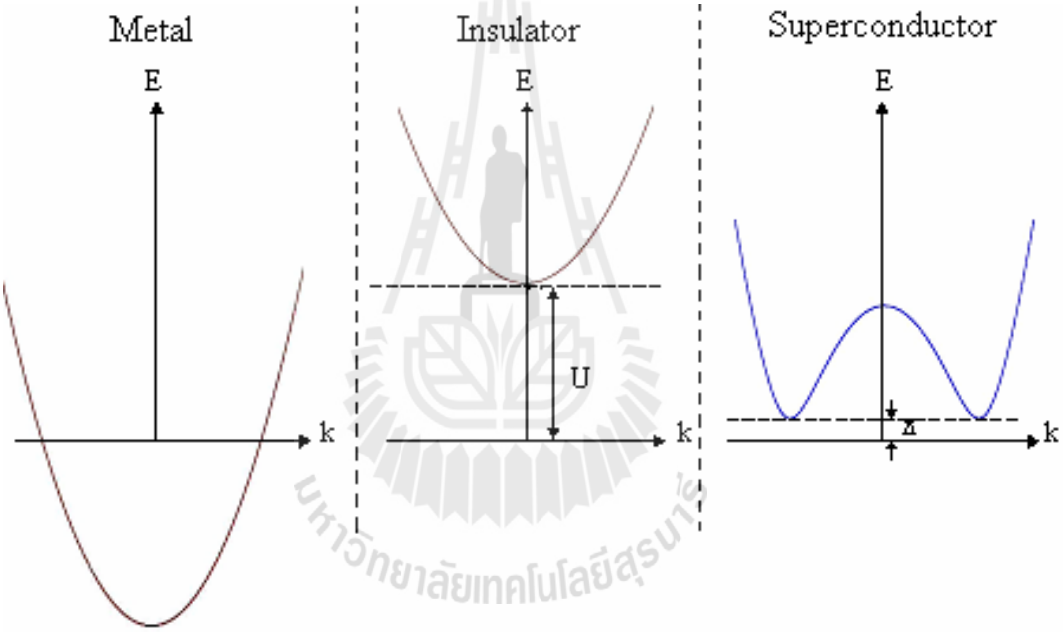

Figure 1.2 The energy dispersion relations of (from left to right) the metal, insulator and superconductor. The Fermi level is set to be in the conduction band of the metal and U below the bottom of the conduction band of the insulator. Δ is the superconducting energy gap.

In calculating the current and conductance of the junctions, the scattering method with the assumption of elastic scattering (Griffin and Demers, 1971; Blonder,

Tinkham, and Klapwijk, 1982) is used. Throughout this study, the effect of finite temperature on the tunneling spectrum is also ignored. The non-zero temperature is expected to smear out sharp features appearing in the tunneling spectrum. Also, each interface of the junctions is assumed to be smooth, i.e., the effect of roughness is not considered.

1.4 Outline of Thesis

This thesis contains the theoretical study of the effect of the insulating layer in MIM and MIS tunneling spectroscopy. The scattering method with two models: Delta-function and Finite-width models, is used to calculate current and conductance spectra of all the junctions. The organization of this thesis is as follows. In Chapter II, the review of the scatter formalism used to obtain the current and conductance of both the MIM and MIS junctions is given. In Chapter III, the current and conductance spectra of MIM from both models are presented and compared. The tunneling spectroscopy of MIS junction from both models are presented and compared in Chapter IV. Finally, the conclusions of this thesis are presented in Chapter V.

CHAPTER II

CURRENT AND CONDUCTANCE IN DELTA-FUNCTION AND FINITE-WIDTH MODELS

In this thesis, two models are considered in studying MIM and MIS junctions: Delta-function model and Finite-width model. In the former model, there are two regions, one parameter characterizing the insulating layer, and one interface. In the latter model, there are three regions, two parameters characterizing the insulating layer and two interfaces. In the scattering method, one needs to obtain the wave functions describing each region of the junctions and use appropriate matching conditions at each interface, in order to get reflection and transmission probabilities, which in turn are used to calculate the tunneling current density and conductance as a function of applied voltage. This chapter contains all the details of how the wave functions in all the regions in each model are obtained, how the suitable matching conditions are used to obtain the reflection and transmission probabilities, and how these probabilities are used to get the tunneling current density and conductance spectra.

2.1 The Two Models

The first model used to study MIM and MIS junctions is called Delta-function model. In this model (see Fig. 2.1), the two metals of MIM junction and the metal and superconductor of MIS junction are located in the region when $x < 0$ and $x > 0$ respectively. The insulating layer is represented by a delta-function barrier potential

described as $H\delta(x)$ where H is the strength of the potential located at $x = 0$. The second model is called Finite-width model. In this model, the insulating layer is modeled by a layer of finite thickness L (see Fig. 2.2). One of the metals occupies the region where $x < 0$ and the other metal or the superconductor occupies the $x > L$ region.

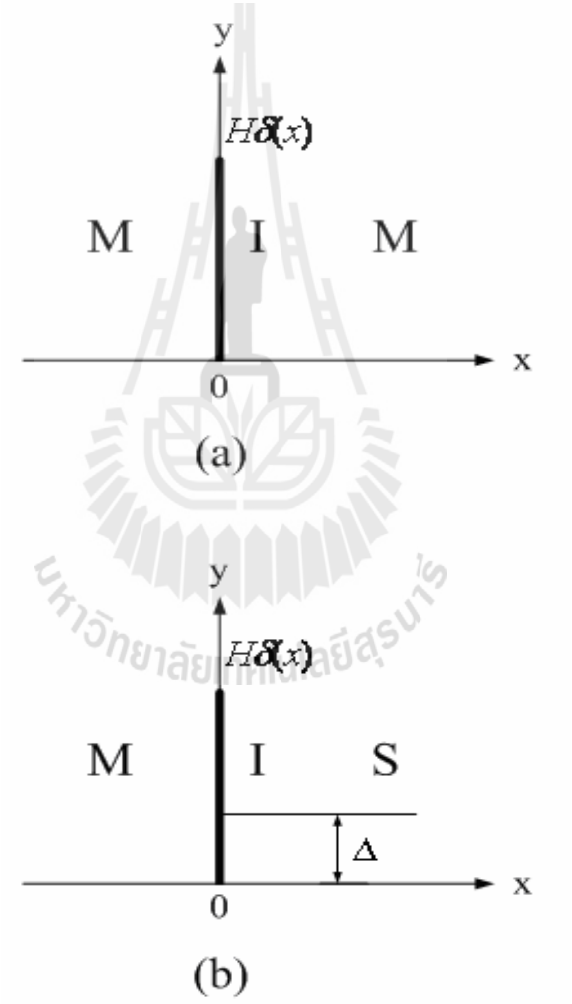

Figure 2.1 The diagrams of Delta-function model. The barrier potential of insulating layer is represented by $H\delta(x)$. (a) is for MIM junction and (b) is for MIS junction. Δ is the superconducting gap.

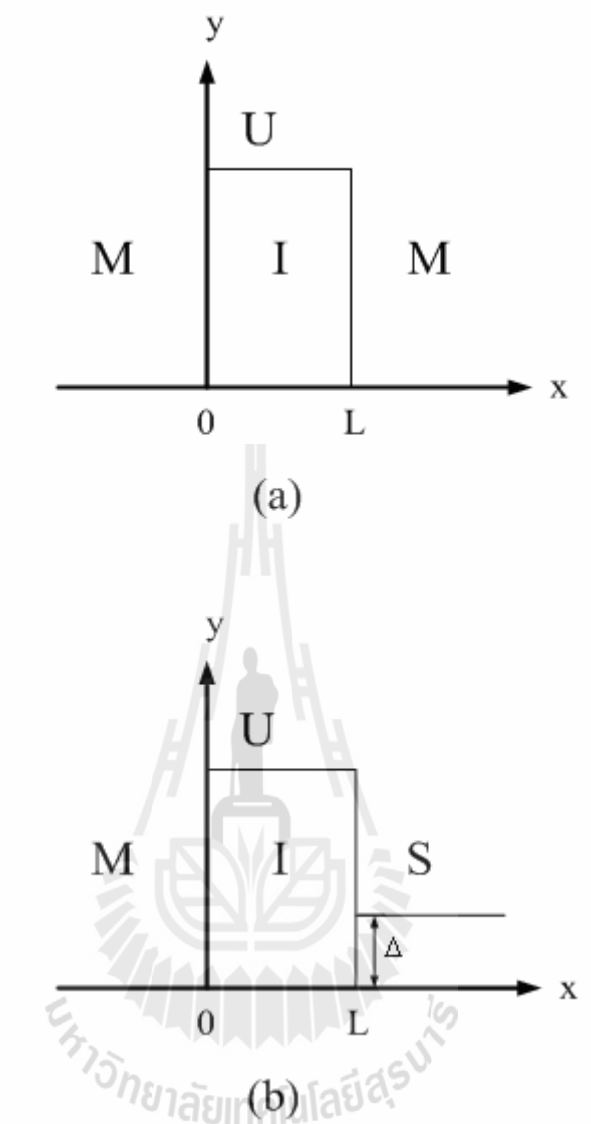

Figure 2.2 The diagrams of the Finite-width model. The insulator is represented by a barrier of thickness *L* and *U*. Δ is the superconducting gap. The figure (a) describes the MIM junction and (b) represents MIS junction.

There are two wave functions describing the particles in the two regions in the Delta-function model and there are three wave functions describing the particles in the three regions in the Finite-width model. How to obtain these wave functions is described in the next section. The matching conditions of the wave functions used in

the former model are the continuity of the wave functions and the discontinuity of the slope of the wave functions at $x = 0$. These conditions lead to two equations to be solved for the reflection and transmission probabilities. In the latter model, the matching conditions are the continuity of the wave functions and of the slope of the wave functions at $x = 0$ and $x = L$. These conditions lead to four equations to be solved for the reflection and transmission probabilities.

2.2 Energy Spectrum and Wave Function in Each Region

2.2.1 MIM Junction

For MIM junction, the time-independent Schrödinger equation is used to describe the system. That is,

$$H_0\psi(x) = E\psi(x) \tag{2.1}$$

where $H_0 = -\frac{\hbar^2}{2m}\frac{d^2}{dx^2} + V(x) - E_F$, $V(x) = H\delta(x)$ in the Delta-function model (where $\delta(x)$ is the Dirac delta function) and $V(x) = U\left(\Theta(x) - \Theta(x-L)\right) + E_F$ in the Finite-width model (where $\Theta(x)$ is the Heaviside step function), E_F is the Fermi energy, m is the electron mass, $\psi(x)$ is the wave function and E is the excitation energy. Note that the Fermi energies of both metals are taken to be the same. The diagrams of energy momentum dispersion relations of both metals are shown in Fig. 2.3.

The excitation energy of each metal is therefore

$$E(k) = \left[\frac{\hbar^2 k^2}{2m} - E_F\right] \tag{2.2}$$

where k is the wave vector.

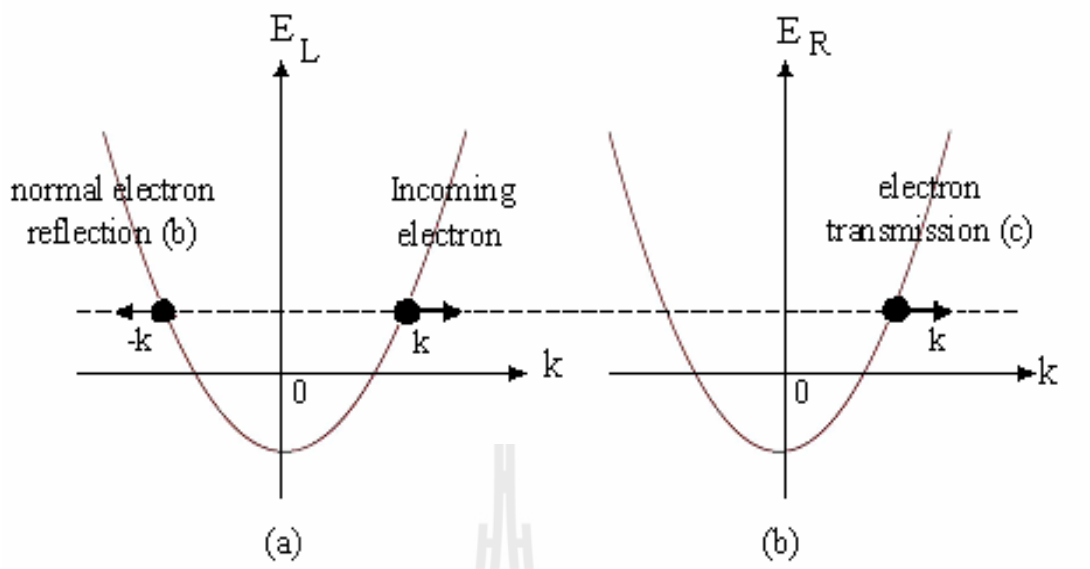

Figure 2.3 The sketches of the energy spectrum of the metal (a) on the left and (b) on the right of MIM junction. The full dots (•) represent the states making up the wave function of each metal.

With the assumption that an electron is injected from the left side of the junction, the suitable wave functions describing the electron of both metals are as follows. The wave function of the electron in the left metal is a linear combination of one incident electron state and the reflected electron state of the same energy:

$$\psi_L(x) = e^{ikx} + be^{-ikx} \tag{2.3}$$

where b is the reflection amplitude. The wave function of the electron in the right metal is

$$\psi_R(x) = ce^{ikx} \tag{2.4}$$

where c is the transmission amplitude. Note that k is always real and $k = \sqrt{\frac{2m}{\hbar^2}(E + E_F)}$.

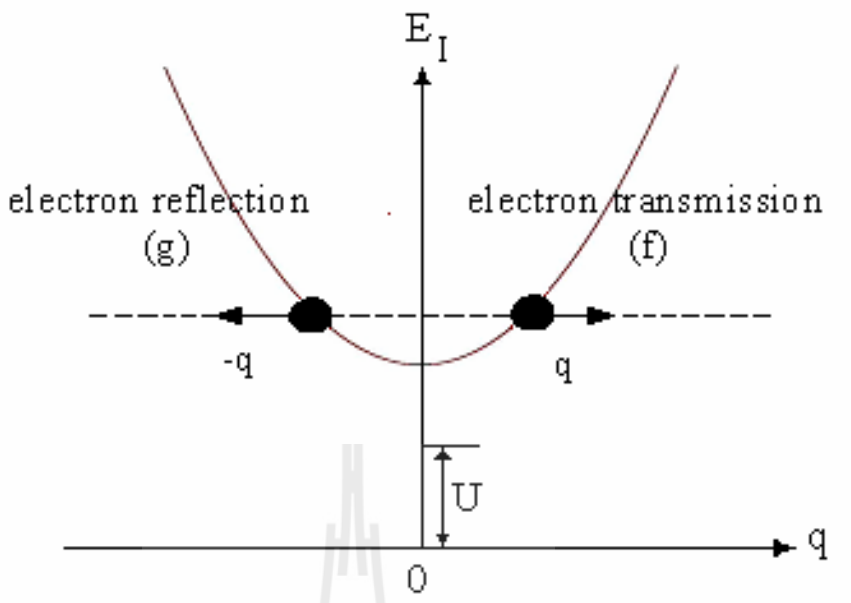

Figure 2.4 The sketch of the energy spectrum in the insulator region. The full dots (•) represent the states making up the wave function in this region.

In the Finite-width model, the excitation energy of the insulator is written as

$$E(q) = \frac{\mathrm{h}^2 q^2}{2m} + U \tag{2.5}$$

where q is the wave vector.

In this region, the wave function of the electron is the sum of the two states of the same energy. That is,

$$\psi_I = fe^{iqx} + ge^{-iqx} \tag{2.6}$$

where f and g are the amplitudes for both states. Note that $q = \sqrt{\frac{2m}{\mathrm{h}^2}(E-U)}$ for $E > U$ and $q = i\sqrt{\frac{2m}{\mathrm{h}^2}(U-E)}$ for $E < U$.

2.2.2 MIS Junction

In order to calculate the tunneling current and conductance spectrum of an MIS junction, one starts from the Bogoliubov-de Gennes (BdG) equations:

$$\begin{pmatrix} H_0 & \Delta(x) \\ \Delta^*(x) & -H^*_0 \end{pmatrix} \psi(x) = E\psi(x) \tag{2.7}$$

where $H_0 = -\frac{\hbar^2}{2m}\frac{d^2}{dx^2} + V(x) - E_F$, $V(x)$ is a potential barrier as defined previously, $\Delta(x) = \Delta\Theta(x)$ in case of Delta-function model and $\Delta(x) = \Delta\Theta(x - L)$ in case of Finite-width system (where Δ is taken to be real) and $\psi(x)$ is a two-component wave function, or $\psi(x) = \begin{bmatrix} u_k \\ v_k \end{bmatrix} e^{ikx}$, where u_k and v_k are the electron-like and hole-like quasiparticle amplitudes respectively. The u_k and v_k are defined as

$$u_k = \frac{E + \xi_k}{\sqrt{|E + \xi_k|^2 + \Delta^2}} \tag{2.8}$$

$$v_k = \frac{\Delta}{\sqrt{|E + \xi_k|^2 + \Delta^2}} \tag{2.9}$$

where $\xi_k = \sqrt{E_k^2 - \Delta^2}$. Again, here the Fermi wave vectors of both metal and superconductor are taken to be the same.

From the BdG equations, the excitation energy of the metal is

$$E(k) = \left[\pm\frac{\hbar^2 k^2}{2m} - E_F \right] \tag{2.10}$$

where k is the wave vector. The upper and lower signs refer to electron and hole energies respectively.

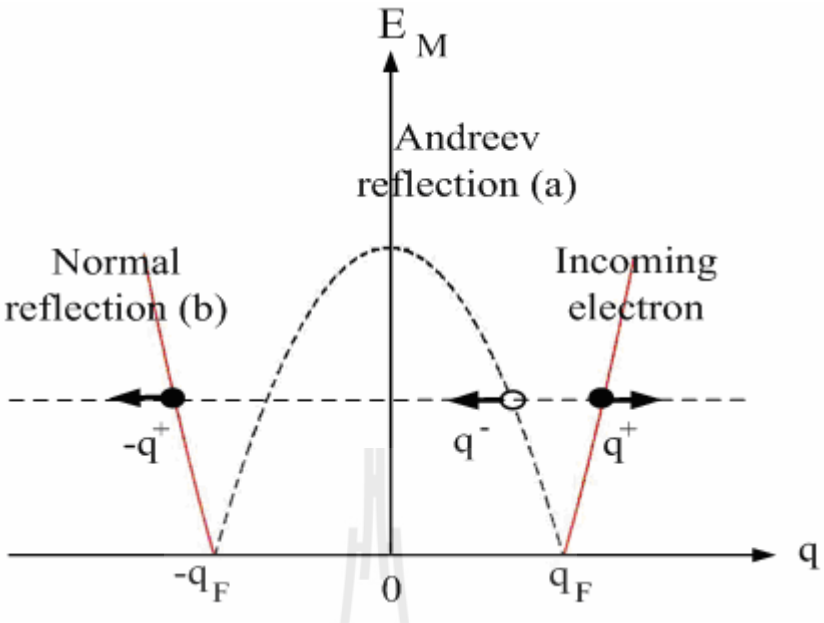

Figure 2.5 The sketch of the energy dispersion relation in the metal region of MIS junction. The solid lines represent electron excitations and the dashed lines represent hole excitations. The full dots (•) and open dot (o) represent electron and hole states that makes up the wave function in this region respectively.

With the assumption that an incident electron comes from the metal side, the wave function of the excitation of metal region is a linear combination of the incident electron, the Andreev reflected hole and the normal reflected electron of the same energy. That is,

$$\psi_L(x) = \begin{bmatrix} 1 \\ 0 \end{bmatrix} e^{ik^+x} + a \begin{bmatrix} 0 \\ 1 \end{bmatrix} e^{ik^-x} + b \begin{bmatrix} 1 \\ 0 \end{bmatrix} e^{-ik^+x} \tag{2.11}$$

where a, b are the Andreev and normal reflection amplitudes respectively. Note that $k^{\pm} = \sqrt{\frac{2m}{\hbar^2}(E_F \pm E)}$.

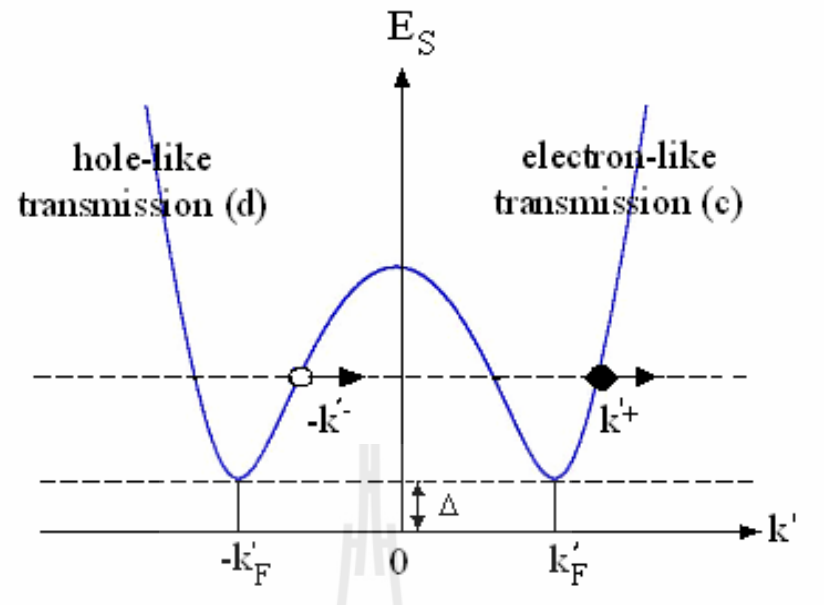

Figure 2.6 The diagram of energy spectrum of the superconductor. The full dot (•) and open dot (o) represent electron-like and hole-like quasiparticles making up the wave function of the superconductor respectively.

In the superconductor region, the wave function of the excitation is a linear combination of two transmitted excitations of the same energy:

$$\psi_S(x) = c\begin{bmatrix} u \\ v \end{bmatrix} e^{ik'^{+}x} + d\begin{bmatrix} v \\ u \end{bmatrix} e^{-ik'^{-}x} \tag{2.13}$$

where c and d are the amplitudes of electron-like and hole-like transmitted quasi-particles respectively. Note that $k'^{\pm} = \sqrt{\frac{2m}{\hbar^2}\left(E_F \pm \sqrt{E^2 - \Delta^2}\right)}$.

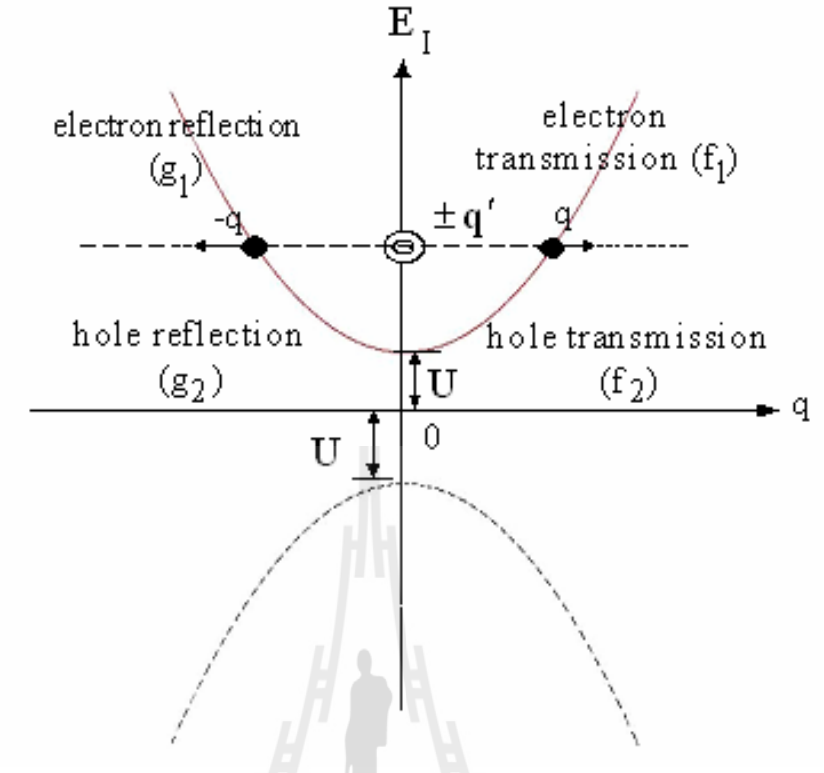

Figure 2.7 Schematic illustration of the energy dispersion relation in the insulating region. The solid line denotes the electron excitation and dashed line represents the hole excitation. The full dots (•) and the open dots (o) denote the states making up the wave function in this region. Note that q' is always pure imaginary.

As for the insulator, the excitation energy is

$$E(q) = \pm\frac{\mathrm{h}^2 q^2}{2m} \pm U \tag{2.14}$$

where the upper and lower signs are for electron and hole excitations respectively.

The wave function of the excitation in the insulating region is

$$\psi_I = f_1\begin{bmatrix}1\\0\end{bmatrix}e^{iqx} + g_1\begin{bmatrix}1\\0\end{bmatrix}e^{-iqx} + f_2\begin{bmatrix}0\\1\end{bmatrix}e^{iq'x} + g_2\begin{bmatrix}0\\1\end{bmatrix}e^{-iq'x} \tag{2.15}$$

where f_1, g_1, f_2 and g_2 are the amplitudes of the electron and hole excitations that make up the wave function in this region. Note that for $E > U$ the wave vector $q = \sqrt{\frac{2m}{\hbar^2}(E-U)}$, for $E < U$ the wave vector $q = i\sqrt{\frac{2m}{\hbar^2}(U-E)}$, and $q' = i\sqrt{\frac{2m}{\hbar^2}(E+U)}$ for all energies.

2.3 Matching Conditions

The appropriate matching conditions at the interface in the Delta-function model are

$$\psi_L(x=0) = \psi_R(x=0) \tag{2.16}$$

$$\frac{d\psi_R}{dx}(x=0) - \frac{d\psi_L}{dx}(x=0) = 2k_F Z\psi_R(x=0) \tag{2.17}$$

where L and R refer to the left side and the right side of the insulting barrier, $Z = \frac{mH}{k_F\hbar^2}$ is a dimensionless parameter representing the insulating barrier strength of the junction (H is the strength of the potential barrier).

In the Finite-width model, the appropriate matching conditions at the two interfaces are

$$\psi_L(x=0) = \psi_I(x=0) \tag{2.18}$$

$$\psi_I(x=L) = \psi_R(x=L) \tag{2.19}$$

$$\frac{d\psi_L}{dx}(x=0) = \frac{d\psi_I}{dx}(x=0) \tag{2.20}$$

$$\frac{d\psi_I}{dx}(x=L) = \frac{d\psi_R}{dx}(x=L) \tag{2.21}$$

where *I*, *L* and *R* refer to the insulating layer, the left side and the right side of the insulting layer respectively.

2.4 Transmission and Reflection Probabilities

In the case of MIM junction, the reflection and transmission probabilities are calculated by assuming that an electron comes from the left region. These probabilities are obtained from the matching conditions described in the previous section.

In the case of MIM junction, the reflection probabilities of the reflected electron $B(E)$ in the both models are equal to the ratio of the current density due to the reflected electron and that of the incident electron. Thus,

$$B(E) = |b(E)|^2 \tag{2.22}$$

similarly, the transmission probability $C(E)$ is

$$C(E) = |c(E)|^2 \tag{2.23}$$

The conservation of the number of particles requires

$$C(E) + B(E) = 1 \tag{2.24}$$

In the case of MIS junction, there are two reflection probabilities, the normal reflection $B(E)$, which has the same form as in Eq. (2.22) and the Andreev reflection $A(E)$ probabilities. $A(E)$ is equal to

$$A(E) = |a(E)|^2 \left| \frac{k^-}{k^+} \right| \tag{2.25}$$

there are also two transmission probabilities. The probability of transmission of the electron-like quasiparticle $C(E)$ is equal to

$$C(E) = |c(E)|^2 \left(|u_k|^2 - |v_k|^2 \right) \left| \frac{k'^+}{k^+} \right| \tag{2.26}$$

and the transmission probability of hole-like quasiparticle $D(E)$ is

$$D(E) = |d(E)|^2 \left(|u_k|^2 - |v_k|^2 \right) \left| \frac{k'^-}{k^+} \right| \tag{2.27}$$

The conservation of the number of particles requires

$$A(E) + B(E) + C(E) + D(E) = 1 \tag{2.28}$$

2.5 Current and Conductance Formulae

The current density tunneling across the junction in the $+x$ direction is given by

$$j^{\rightarrow} = \sum_k n_k v_k e = \frac{eL}{2\pi} \int dk \; n_k v_k \tag{2.29}$$

where n_k is number of electron tunneling across the junction, which is equal to $n_k = T(E) f(E)$, where $T(E)$ is the total electron transmission probability and $f(E)$ is the Fermi-Dirac distribution function, and the group velocity $v_k = \frac{1}{\mathrm{h}} \frac{dE}{dk}$. Note that the sum or the integration is over all the states with the positive group velocities. For an MIM junction, $T(E) = 1 - B(E)$ and for an MIS junction, $T(E) = 1 + A(E) - B(E)$. From Eq. (2.29), by changing the integration variable from k to E, one obtains,

$$j^{\rightarrow} = \frac{Le}{2\pi \mathrm{h}} \int_{-\infty}^{\infty} dE \; T(E) f(E) \tag{2.30}$$

when there is no applied voltage across the junction, the net current density is zero; that is, the current density flowing to the right is equal to the left:

$$j^{\rightarrow} = j^{\leftarrow} = \frac{Le}{2\pi \mathrm{h}} \int_{-\infty}^{\infty} dE \; T(E) f(E) \tag{2.31}$$

when there is a positive applied voltage V across the junction, the current density to the right becomes

$$j^{\rightarrow} = \frac{Le}{2\pi \mathrm{h}} \int_{-\infty}^{\infty} dE\ T(E) f(E - eV) \tag{2.32}$$

therefore, the net current density at this voltage is

$$j_{net}{}^{\rightarrow} = j^{\rightarrow} - j^{\leftarrow} = \frac{Le}{2\pi \mathrm{h}} \int_{-\infty}^{\infty} dE\ T(E)\big(f(E - eV) - f(E)\big) \tag{2.33}$$

at zero temperature, the net current density becomes

$$j_{net}{}^{\rightarrow}(eV, T = 0) = \frac{Le}{2\pi \mathrm{h}} \int_{0}^{eV} dE\ T(E) \tag{2.34}$$

the conductance is the derivative of current density with respect to the applied voltage:

$$G(eV) = \frac{dj_{net}{}^{\rightarrow}}{dV} \tag{2.35}$$

Thus, at zero temperature, the conductance of MIM and MIS junctions are

$$G_{\mathrm{MIM}}(eV) = \frac{e^2}{\mathrm{h}} \frac{L}{2\pi} \big(1 - B(eV)\big) \tag{2.36}$$

$$G_{\mathrm{MIS}}(eV) = \frac{e^2}{\mathrm{h}} \frac{L}{2\pi} \big(1 + A(eV) - B(eV)\big) \tag{2.37}$$

respectively.

CHAPTER III

MIM TUNNELLING SPECTROSCOPY

The current density and conductance spectra of MIM junction obtained from the Delta-function model and the Finite-width model are shown and discussed in this chapter. As already mentioned in the previous chapter, the junction is represented by a one-dimensional infinite system in both models. The Fermi wave vectors of both metals are assumed to have the same magnitude.

In the Delta function model, the effect of the insulating barrier, which is characterized by the parameter Z (as defined as $Z = \frac{mH}{k_F \mathrm{h}^2}$ is a dimensionless parameter), on both current density and conductance spectra are investigated. Similarly, in the Finite-width model, the dependence of the current density and conductance spectra on the insulating barrier, which is characterized by the two parameters U (the barrier potential) and L (the width of the barrier), is studied.

For simplicity, the effect of finite temperature is not considered. The finite temperature is expected not to affect the positions of the main features in both current density and conductance spectra.

3.1 Delta-Function Model

The plots of both the current density and conductance as a function of applied voltage in the Delta-function model are illustrated in Fig. 3.1.

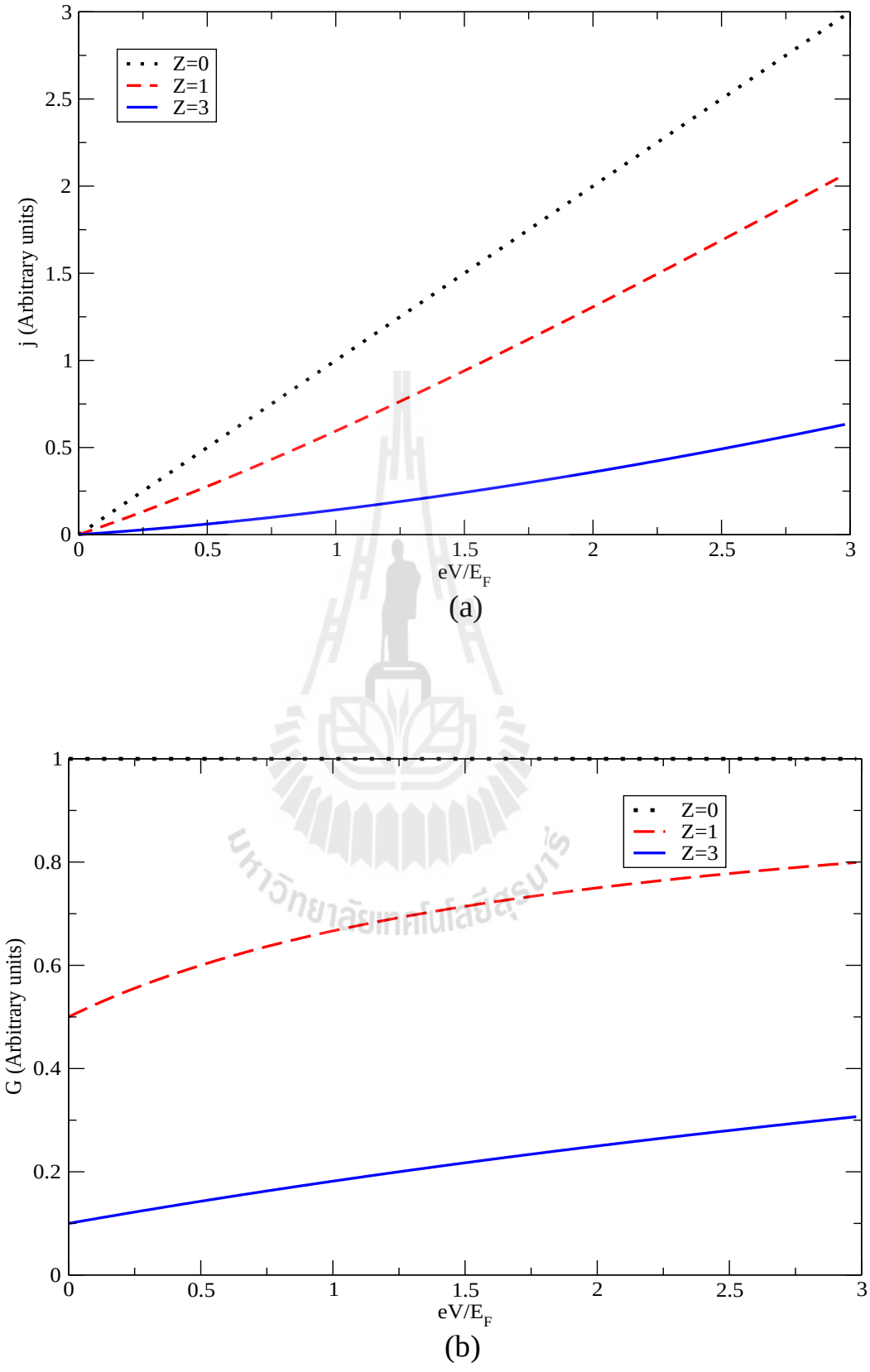

Figure 3.1 The plots of (a) current density *j* and (b) conductance *G* as a function of applied voltage at different values of parameter Z: *Z* = 0, 1 and 3.

The current density and the conductance are found to be

$$j(eV) = \frac{Le}{2\pi}\int_0^{eV}\left(\frac{E+E_F}{E+E_F\left(1+Z^2\right)}\right)dE \tag{3.1}$$

$$G(eV) = \frac{Le^2}{2\pi\mathrm{h}}\left(\frac{eV+E_F}{eV+E_F\left(1+Z^2\right)}\right) \tag{3.2}$$

As can be seen in Fig. 3.1, when there is no barrier strength (Z = 0), it is not surprising to get the conductance plot to be equal to 1. When Z is non-zero and becomes bigger, the current flowing through the junction gets smaller and so does the conductance.

3.2 The Finite-Width Model

In this model the expressions of the current density and the conductance are more complicated than in the Delta-function model. That is,

For $E < U$,

$$j(eV) = \frac{Le}{2\pi}\int_0^{eV}\left(\frac{1}{1+\frac{1}{4}\left(\frac{(U+E_F)^2}{(E+E_F)(U-E)}\right)\sinh^2\left(\sqrt{\frac{1}{E_F}(U-E)}\right)Lk_F}\right)dE \tag{3.3}$$

$$G(eV) = \frac{Le^2}{2\pi\mathrm{h}}\left(\frac{1}{1+\frac{1}{4}\left(\frac{(U+E_F)^2}{(eV+E_F)(U-eV)}\right)\sinh^2\left(\sqrt{\frac{1}{E_F}(U-eV)}\right)Lk_F}\right) \tag{3.4}$$

For $E > U$,

$$j(eV) = \frac{Le}{2\pi}\int_0^{eV}\left(\frac{1}{1+\frac{1}{4}\left(\frac{(U+E_F)^2}{(E+E_F)(E-U)}\right)\sin^2\left(\sqrt{\frac{1}{E_F}(E-U)}\right)Lk_F}\right)dE \qquad (3.5)$$

$$G(eV) = \frac{Le^2}{2\pi\mathrm{h}}\left(\frac{1}{1+\frac{1}{4}\left(\frac{(U+E_F)^2}{(eV+E_F)(eV-U)}\right)\sinh^2\left(\sqrt{\frac{1}{E_F}(eV-U)}\right)Lk_F}\right) \qquad (3.6)$$

Figures 3.2 - 3.3 show the current density and conductance spectra as a function of applied voltage in the model. The both spectra show strong dependence on the barrier potential and the thickness of the insulator.

As can be seen from Fig. 3.2 (a), when the insulating layer is thick and the applied voltage is less than the barrier potential, there is very small tunneling current density flowing across the junction. When the voltage is higher than the potential, the current density starts increasing steadily and there is an oscillation with an increasing period as well. These oscillations can be seen more apparently in the conductance spectra as seen in Figs. 3.2 (b) and 3.3 (b). The amplitudes of the oscillations are decreased as the applied voltage is increased.

When the insulating thickness is varied, it can be seen in Fig. 3.3 (a) that for thin barrier (Lk_F = 1) the tunneling current density is non-zero even when the applied voltage is less than the barrier potential, and it is increased with the applied voltage. This non-zero current is due to the fact that when the insulating layer is thin, only a small decay in the magnitude of the wave function in the insulating region occurs. The oscillations in the current density cannot be seen clearly in the case where the barrier

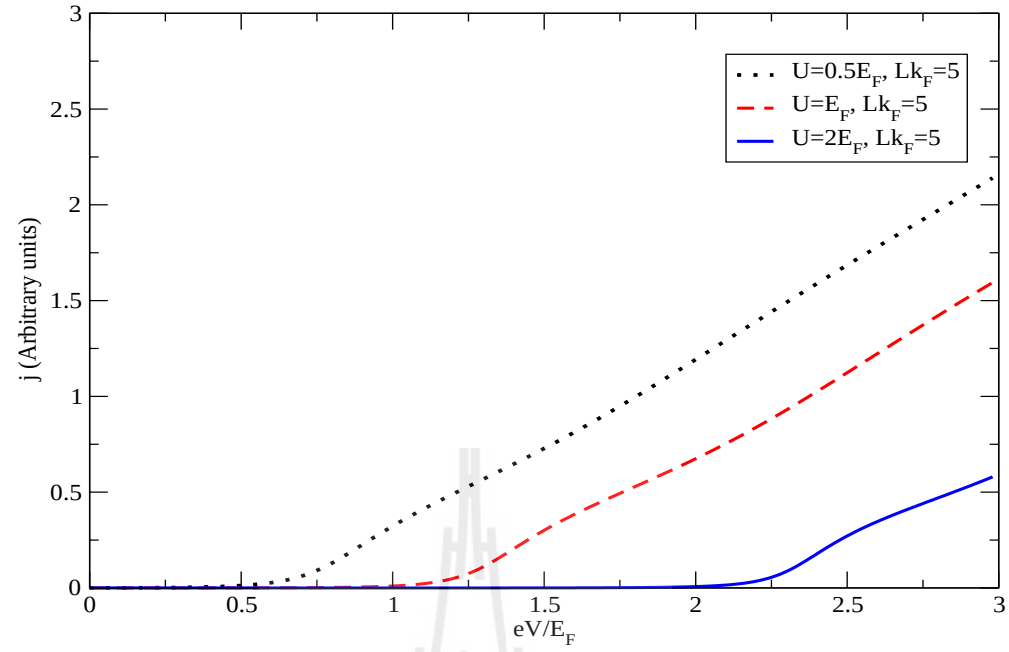

(a)

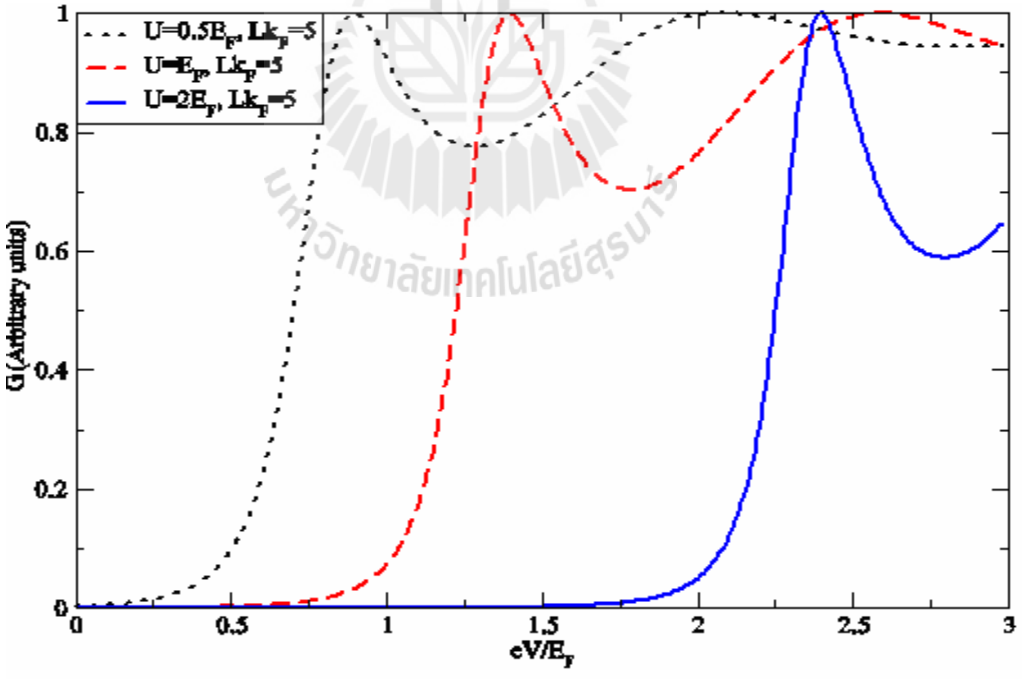

(b)

Figure 3.2 The plots of (a) current density j and (b) conductance G as a function of applied voltage at different the barrier potential U = 0.5 E_F, E_F and 2 E_F, when the thickness Lk_F = 5.

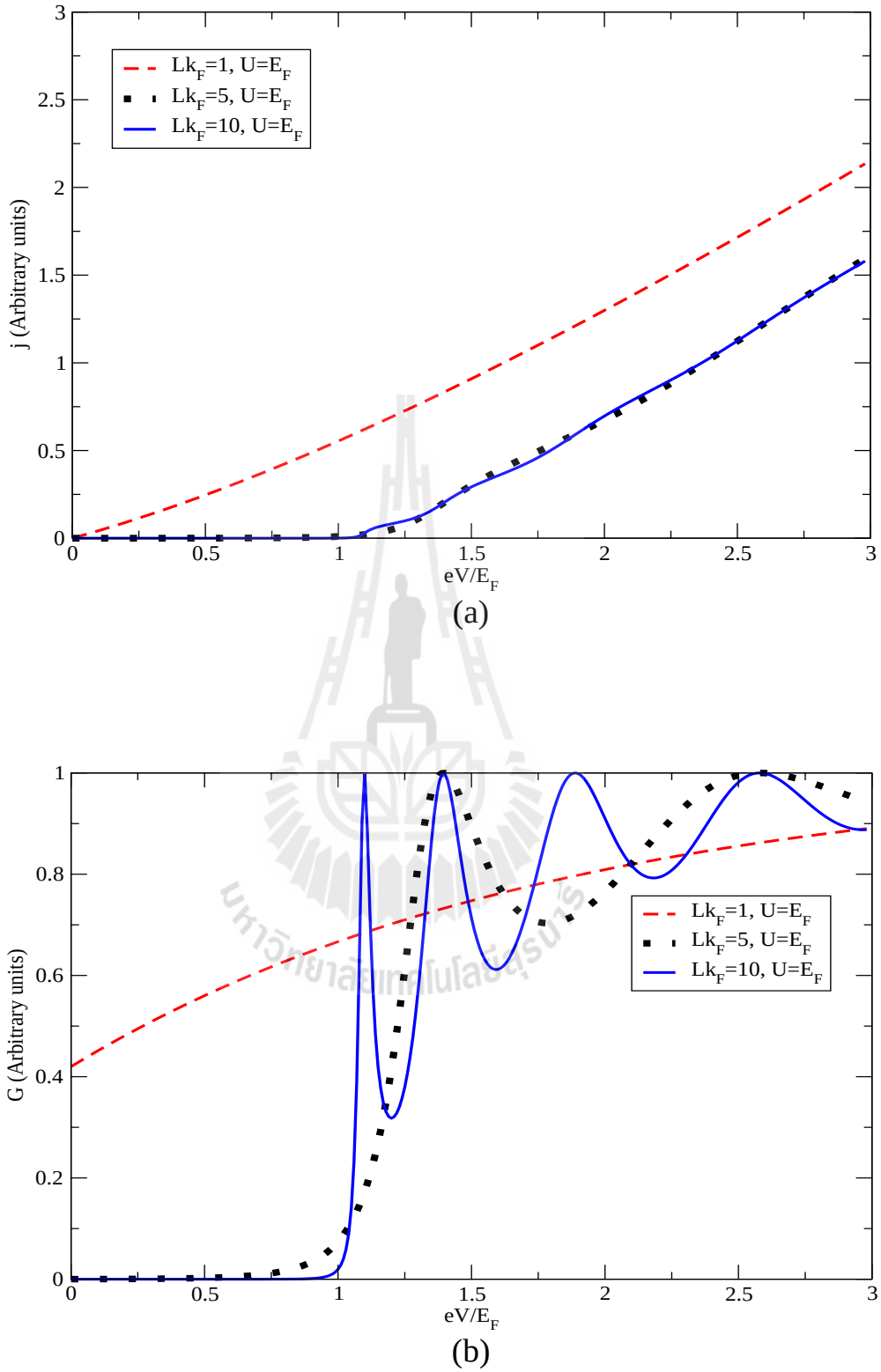

Figure 3.3 The plots of (a) current density j and (b) conductance G as a function of applied voltage at different the thickness Lk_F = 1, 5 and 10, when the potential barrier $U = E_F$.

thickness is too small.

When the barrier is thick, as mentioned in the previous paragraph, the tunneling current density is very small when the applied voltage is less than the barrier potential. The oscillation in the current density spectrum is more apparent, when the thickness is large enough. These oscillating features are prominent in the conductance spectrum (Fig. 3.3 (b)) and the period of the oscillation is smaller for a thicker insulating layer.

The period of the oscillations is associated with the properties of the insulating layer. It corresponds to the difference between the two adjacent energy levels of the electrons in the insulating layer of thickness L. The energy levels of an electron in the insulating layer of thickness L in vacuum can be found to be

$$E_n = U + \frac{\mathrm{h}^2}{2m}\left(\frac{n\pi}{L}\right)^2 \tag{3.7}$$

where n = 1, 2, 3, … . When the insulating layer is sandwiched between two metals, these energy levels coincide with the applied voltage where the transmission probability is the highest and can be seen as the maxima in the conductance spectrum. The distance in applied voltage between the adjacent maxima is

$$\Delta E_n = \frac{\mathrm{h}^2}{2m}\left(\frac{\pi}{L}\right)^2 (2n+1) \tag{3.8}$$

which is increased with the energy level n and is decreased with the thickness L.

3.3 Comparison and Equivalency of the Two Models

It is obvious that the Finite-width model is more realistic in representing the

real system. It provides more information about the insulating layer than the Delta-function model. However, the calculation in the Finite-width model, which is involved three regions and two parameters characterizing the insulating barrier, is much more complicated than that in the Delta-function model, which is involved two regions and only one parameter for the barrier. As already shown in the previous section, in the Finite-width model one can see the oscillation occurring in both current density and conductance spectra at the voltage higher than the barrier potential. This feature cannot be seen if one uses the Delta-function model to represent the junction.

The current density and conductance spectra in the Delta-function model are similar to those in the Finite-width model when the applied voltage is less than the barrier potential and where the thickness L of the insulator region is small. This similarity suggests that as long as the insulating layer of the junction is thin enough, one may use the Delta-function model in place of the Finite-width model. Now the question is how thick is thin enough. To answer the question, one can compare the value of the conductance at zero voltage from the two models. The conductance at zero voltage from the Delta-function model is

$$G_D(eV = 0, Z) = \frac{1}{Z^2 + 1} \tag{3.9}$$

the conductance at zero voltage from the Finite-width model is

$$G_F(eV = 0, L, U) = \frac{1}{1 + \frac{1}{4}\left(\frac{(U + E_F)^2}{UE_F}\right)\sinh^2\left(\left(\sqrt{\frac{U}{E_F}}\right)Lk_F\right)} \tag{3.10}$$

where k_F and E_F are the Fermi wave vector and the Fermi energy of the metal region.

In the limit where $\left(\sqrt{U/E_F}\right)Lk_F << 1$, one can find the relationship between

the insulating parameters of the two models by approximating $\sinh(x) \approx x$ for $x << 1$ and equating the two equations above. The relation is,

$$Z = \frac{(U + E_F)}{2E_F} Lk_F \tag{3.11}$$

which reflects the equivalency of the two models. The Delta-function model with the parameter Z as shown in the equation above can lead to the same results as the Finite-width model with the equivalent U and L with the condition $\left(\sqrt{U / E_F}\right) Lk_F << 1$. To be more specific, one can show that Eq. (3.11) can be used within 10% accuracy as long as the insulating layer is

$$Lk_F \leq \sqrt{\frac{2E_F^{3/2}}{3\sqrt{U}(U + E_F)}} \tag{3.12}$$

Note that when the barrier potential is high, the thickness must be very thin.

Figs. 3.4 – 3.5 show the plots of the current density and conductance spectra from both models using the insulating parameters according to Eq. (3.11) and the condition (3.12).

As can be seen from Figs. 3.4 - 3.5, both current density and conductance spectra from the two models lie on top of each other within 10% accuracy. The results get worse as the thickness L gets larger or the potential gets bigger. It is worth noted that the bigger value of L affects the similarities of the two models more than the higher barrier potential.

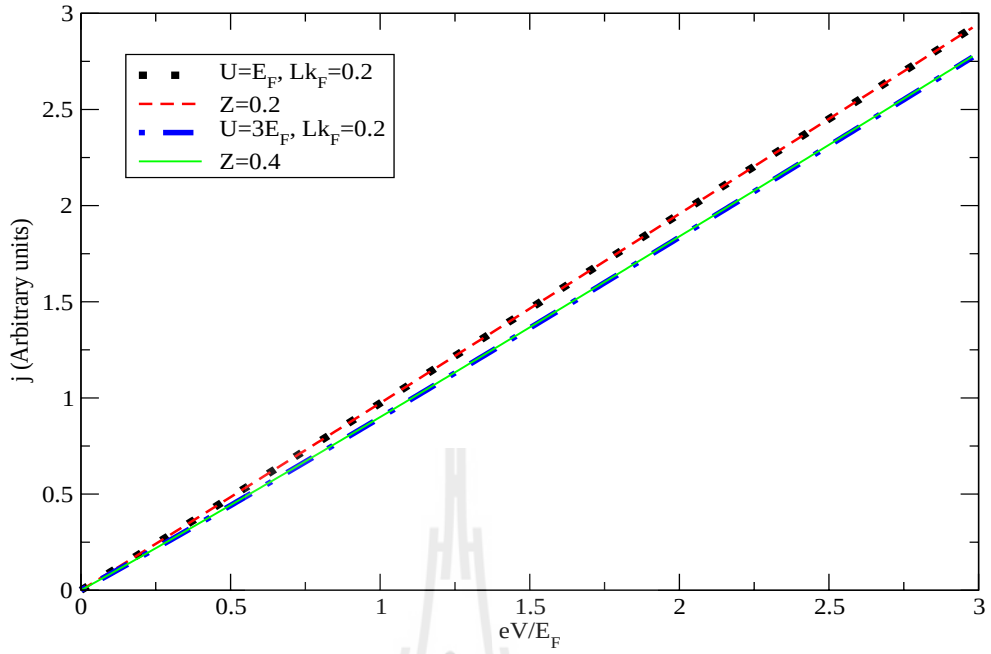

(a)

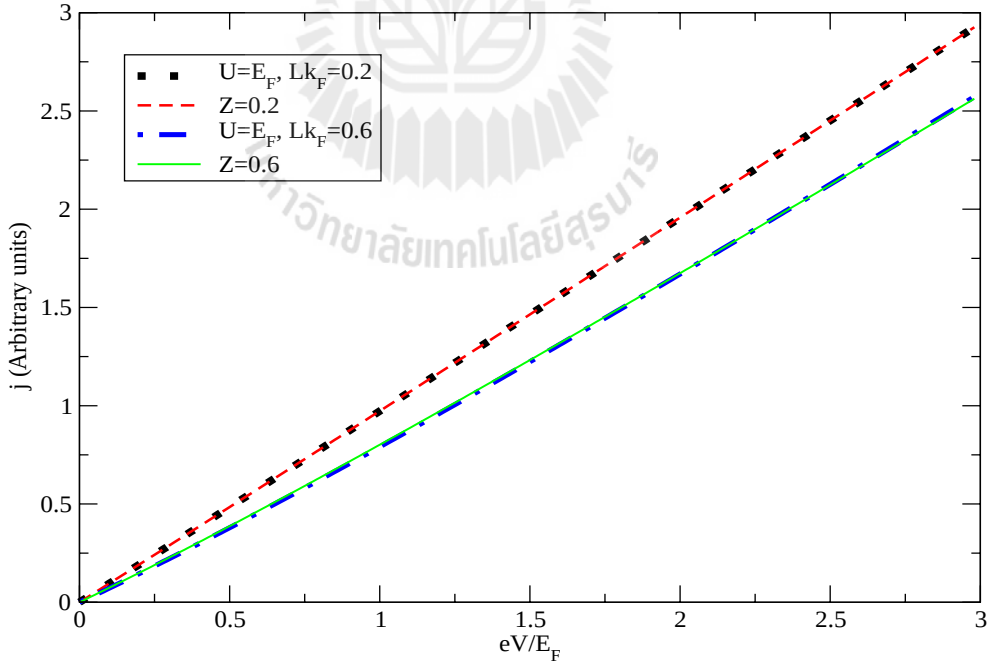

(b)

Figure 3.4 The plot of current density spectra with (a) thickness $Lk_F = 0.2$ (for $U = E_F$, $Z = 0.2$ and for $U = 3E_F$, $Z = 0.4$) and (b) the barrier potential $U = E_F$ (for $Lk_F = 0.2$, $Z = 0.2$ and for $Lk_F = 0.6$, $Z = 0.6$).

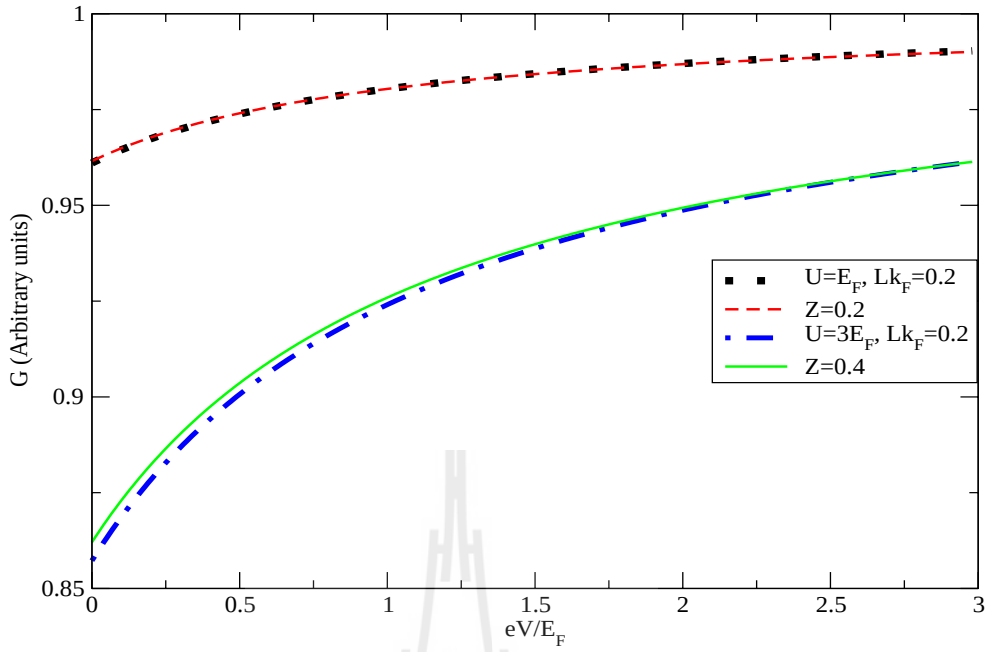

(a)

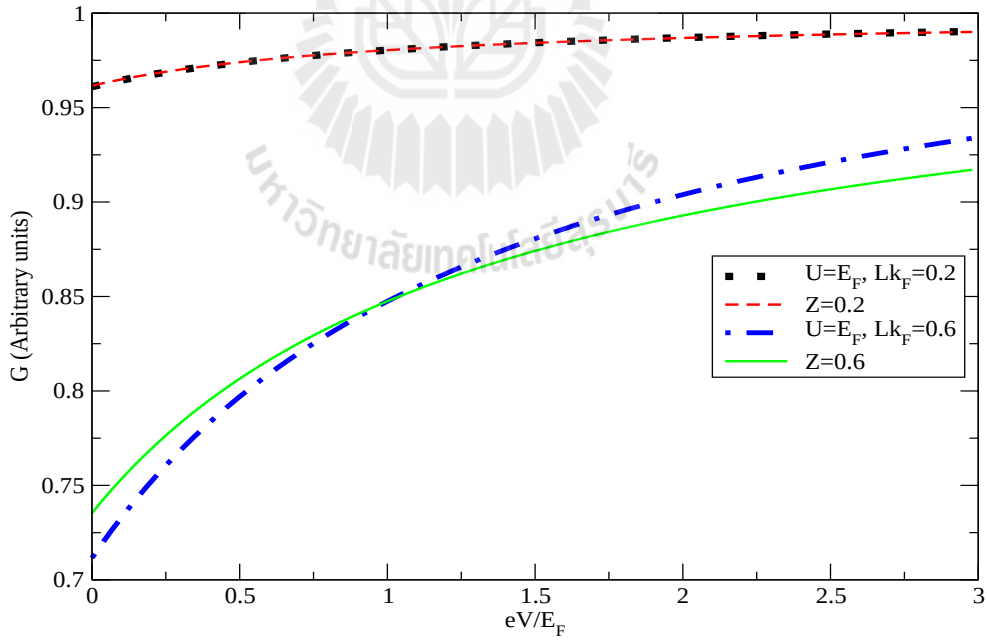

(b)

Figure 3.5 The plot of conductance spectra with (a) thickness Lk_F = 0.2 (for U = E_F, Z = 0.2 and for U = 3 E_F, Z = 0.4) and (b) the barrier potential U = E_F (for Lk_F = 0.2, Z = 0.2 and for Lk_F = 0.6, Z = 0.6).

3.4 Conclusions

The current density and conductance spectra of MIM junction in the Delta-function and Finite-width models are presented in this chapter. The Delta-function model is a simple model as it involves a fewer number of regions and only one parameter charactering the insulating layer. This simplicity limits the results of the Delta-function model to be valid only when the applied voltage is smaller than the barrier potential and the thickness of the insulating layer is small. The current density and conductance spectra obtained from the Finite-width model contain oscillations when the applied voltage is higher than the barrier potential. The periods of the oscillations are not constant and depend on the thickness of the barrier. One learns from these results that as long as the main features, of interest, do not occur at higher energy scale than the barrier potential and the insulating layer is made thin enough, the Delta-function model can be used to study MIM junctions and the parameter Z can be related to U and L according to Eq. (3.11).

In the next chapter, the current density and conductance spectra of MIS junctions are considered. The similar relationships of the insulating parameters of the two models are also obtained.

CHAPTER IV

MIS TUNNELLING SPECTROSCOPY

In this chapter, the effect of the insulating layer on the tunneling spectroscopy of MIS junction in the both Delta-function and Finite-width models are considered. In particular, in the Delta-function model, how the electric current density and conductance spectra are affected by Z, the parameter characterizing the insulator, is reviewed. In the Finite-width model, the effect of the thickness L and the barrier potential U of the insulating barrier is investigated. The results from both models are discussed in details and, similar to MIM junction in the previous chapter, the condition when the Delta-function model can be used in place of the Finite-width model is also given in this chapter.

Throughout this chapter, the calculations are also limited to one-dimensional system in both models and the current density and conductance spectra are those at zero temperature. The Fermi wave vectors of both metal and superconductor are assumed to have the same magnitude.

4.1 Delta-Function Model

In this model, the normal reflection probability $B(E)$ is found to be

$$B(E) = \frac{|u_k(E)|^4 W_1(E) W_3(E) + |v_k(E)|^4 W_2(E) W_5(E)}{|u_k(E)|^4 W_1(E) W_4(E) + |v_k(E)|^4 W_2(E) W_6(E)} \tag{4.1}$$

and the Andreev reflection probability $A(E)$ is

$$A(E)=\frac{4k^{+}(E)k^{-}(E)\left|u_k(E)\right|^2\left|v_k(E)\right|^2(k'^{+}(E)+k'^{-}(E))^2}{\left|u_k(E)\right|^4 W_1(E)W_4(E)+\left|v_k(E)\right|^4 W_2(E)W_6(E)} \tag{4.2}$$

when $W_1(E)$, $W_2(E)$, $W_3(E)$, $W_4(E)$, $W_5(E)$ and $W_6(E)$ are defined as

$$W_1(E)=\left(\left(k'^{-}(E)+k^{-}(E)\right)^2+4k_F^2Z^2\right) \tag{4.3}$$

$$W_2(E)=\left(\left(k'^{+}(E)-k^{-}(E)\right)^2+4k_F^2Z^2\right) \tag{4.4}$$

$$W_3(E)=\left(k^{+}(E)-k'^{+}(E))^2+4k_F^2Z^2\right) \tag{4.5}$$

$$W_4(E)=\left(k^{+}(E)+k'^{+}(E))^2+4k_F^2Z^2\right) \tag{4.6}$$

$$W_5(E)=\left(k^{+}(E)+k'^{-}(E))^2+4k_F^2Z^2\right) \tag{4.7}$$

$$W_6(E)=\left(k^{+}(E)-k'^{-}(E))^2+4k_F^2Z^2\right) \tag{4.8}$$

where $k^{+}(E)$, $k^{-}(E)$, $k'^{+}(E)$, $k'^{-}(E)$, $u_k(E)$ and $v_k(E)$ are $k^{\pm}(E)=\sqrt{\frac{2m}{\hbar^2}(E_F\pm E)}$,

$k'^{\pm}(E)=\sqrt{\frac{2m}{\hbar^2}\left(E_F\pm\sqrt{E^2-\Delta^2}\right)}$, $u_k(E)=\frac{E+\sqrt{E^2-\Delta^2}}{\sqrt{\left|E+\sqrt{E^2-\Delta^2}\right|^2+\Delta^2}}$,

$v_k(E)=\frac{\Delta}{\sqrt{\left|E+\sqrt{E^2-\Delta^2}\right|^2+\Delta^2}}$.

Since the range of energy of interest in MIS tunneling spectroscopy is in the same order of the superconducting gap, which is much less than the Fermi energy, the following approximations are used: $k'^{+}=k'^{-}=k'_F$ and $k^{+}=k^{-}=k_F$. k'_F and k_F are taken to be the same. The inequality of the magnitude of both Fermi wave vectors affects the current density and conductance spectra in the same way as when Z is increased (Blonder and Tinkham, 1983).

With these approximations and assumptions, one gets

$$B(E)=\frac{\left(\left|u_k(E)\right|^2-\left|v_k(E)\right|^2\right|\right)^2\left(Z^2+Z^4\right)}{\left(Z^2(\left|u_k(E)\right|^2-\left|v_k(E)\right|^2)+\left|u_k(E)\right|^2\right)^2} \tag{4.9}$$

Note that when $E < \Delta$, $B(E)$ becomes

$$B(E)=\frac{4\left(Z^2+Z^4\right)\left(\Delta^2-E^2\right)}{E^2+\left(\Delta^2-E^2\right)\left(2Z^2+1\right)^2} \tag{4.10}$$

and when $E \geq \Delta$, one obtains

$$B(E)=\frac{4\left(Z^2+Z^4\right)\left(E^2-\Delta^2\right)}{E^2+\left(E^2-\Delta^2\right)\left(2Z^2+1\right)^2} \tag{4.11}$$

As for the Andreev reflection probability, one obtains

$$A(E)=\frac{\left|u_k(E)\right|^2\left|v_k(E)\right|^2}{\left(Z^2(\left|u_k(E)\right|^2-\left|v_k(E)\right|^2)+\left|u_k(E)\right|^2\right)^2} \tag{4.12}$$

When $E < \Delta$, $A(E)$ is

$$A(E)=\frac{\Delta^2}{E^2+\left(\Delta^2-E^2\right)\left(2Z^2+1\right)^2} \tag{4.13}$$

and when $E \geq \Delta$, $A(E)$ is equal to

$$A(E)=\frac{\Delta^2}{E^2+\left(E^2-\Delta^2\right)\left(2Z^2+1\right)^2} \tag{4.14}$$

As can be seen from Eq. (4.10), when Z is small, the probability of normal reflection is small for $E < \Delta$, whereas the Andreev reflection probability is close to 1. That is, for a transparent barrier, the transfer of electron when $E < \Delta$ is dominated by the two-particle process, i.e., for one incident electron, there can be two transmitted

electrons. In case of large Z, the normal reflection probability is $B(E) \approx 1 - \frac{E}{\sqrt{(E^2 - \Delta^2)Z^2}}$ and the Andreev reflection probability is $A(E) \approx \frac{\Delta^2}{(E^2 - \Delta^2)4Z^2}$.

Thus, the current density as a function of applied voltage at zero temperature is

$$j(eV) = \frac{Le}{2\pi} \int_0^{eV} dE \left(1 + \frac{\Delta^2 - 4(Z^2 + Z^4)|E^2 - \Delta^2|}{E^2 + |E^2 - \Delta^2|(2Z^2 + 1)^2} \right) \tag{4.15}$$

and the conductance is

$$G(eV) = \frac{e^2}{\mathrm{h}} \frac{L}{2\pi} \left(1 + \frac{\Delta^2 - 4(Z^2 + Z^4)|(eV)^2 - \Delta^2|}{(eV)^2 + |(eV)^2 - \Delta^2|(2Z^2 + 1)^2} \right) \tag{4.16}$$

In Fig. 4.1, the current density and conductance as a function of applied voltage at different values of Z are shown.

The results obtained here are consistent with those from the previous work by Blonder, Tinkham and Klapwijk (Blonder, Tinkham, and Klapwijk, 1982). In the case where Z is small, there is excess current due to Andreev reflection, which results in higher value of the conductance when $eV < \Delta$ than that of the conductance when $eV > \Delta$. In the case where Z is large, there is a small tunneling current when $eV < \Delta$. When $eV > \Delta$, the current is increased linearly. These features in the current spectrum cause the conductance spectrum to have the same shape as the density of states of the superconductor.

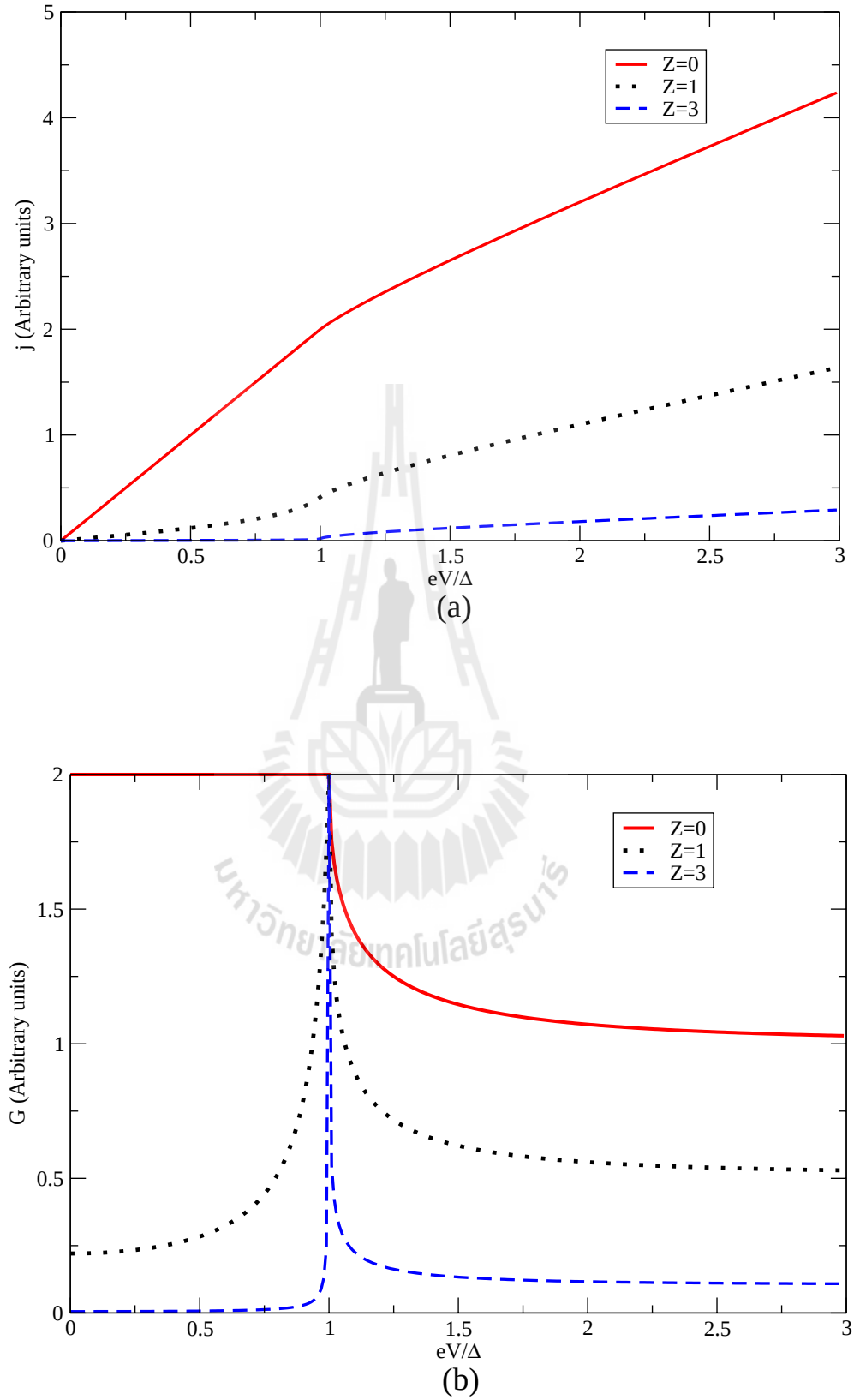

Figure 4.1 The plots of (a) current density j and (b) conductance G as a function of applied voltage. The different values of Z are 0, 1 and 3.

4.2 Finite-Width Model

In this model, both normal reflection probabilities are expressed in much more complicated formulae than those in the Delta-function model. After using the approximations $k^{+} = k^{-} = k_F$, $k'^{+} = k'^{-} = k'_F$ and assume $k'_F = k_F$, one obtains the following expressions for both reflection probabilities.

For $E < U$,

$$B(E) = M_1(E)\left(C(E)\left|u_k(E)\right|^2 + D(E)\left|v_k(E)\right|^2 + \frac{4k_F^2 e^{2q(E)L}}{(q(E)^2 + k_F^2)} \right) + 1 \quad (4.17)$$

$$A(E) = \frac{\left|q'(E)\right|^2 \left(C(E)\left|v_k(E)\right|^2 + D(E)\left|u_k(E)\right|^2 \right)}{\left|q'(E)\right|^2 \cosh^2\left|q'(E)\right|L + k_F^2 \sinh^2\left|q'(E)\right|L} \quad (4.18)$$

where $C(E)$ and $D(E)$ are the probabilities of the electron-like and hole-like quasi-particle, respectively. These probabilities are defined as

$$C(E) = \frac{4k_F^2\left|u_k(E)\right|^2 q(E)^2 \left[\left(\left|q'(E)\right|^2 + k_F^2 \right)^2 \sinh^2\left|q'(E)\right|L + 4k_F^2\left|q'(E)\right|^2 \right]}{M_2(E) + M_3(E)} \quad (4.19)$$

$$D(E) = \frac{4k_F^2\left|v_k(E)\right|^2 q(E)^2 \left[\left(\left|q'\right|^2 + k_F^2 \right)^2 \sinh^2\left|q'(E)\right|L \right]}{M_2(E) + M_3(E)} \quad (4.20)$$

where $M_1(E)$, $M_2(E)$ and $M_3(E)$ are

$$M_1(E) = \left(\frac{q(E)^2}{q(E)^2 \cosh^2 q(E)L + k_F^2 \sinh^2 q(E)L} \right) \quad (4.21)$$

$$\begin{aligned} M_2(E) = \left|u_k(E)\right|^4 & \left[\left(q(E)^2 + k_F^2 \right)^2 \sinh^2 q(E)L + 4k_F^2 q(E)^2 \right] \\ & \times \left[\left(\left|q'(E)\right|^2 + k_F^2 \right)^2 \sinh^2\left|q'(E)\right|L + 4k_F^2\left|q'(E)\right|^2 \right] \end{aligned} \quad (4.22)$$

$$M_3(E) = |v_k(E)|^4 \left[\left(q(E)^2 + k_F^2 \right)^2 \sinh^2 q(E) L \right] \times \left[\left(|q'(E)|^2 + k_F^2 \right)^2 \sinh^2 |q'(E)| L \right] \quad (4.23)$$

where the wave vector $q(E)$ and $q'(E)$ in this case are $q(E) = \sqrt{\frac{2m}{\hbar^2}(U - E)}$ and $q'(E) = i\sqrt{\frac{2m}{\hbar^2}(E + U)}$.

For $E > U$,

$$B(E) = N_1(E) \left(C(E) |u_k(E)|^2 + D(E) |v_k(E)|^2 - \frac{4k_F^2}{(q^2(E) + k_F^2)} \right) + \frac{|k_F - q(E)|^2}{|k_F + q(E)|^2} \quad (4.24)$$

$$A(E) = \frac{|q'(E)|^2 \left(C(E) |v_k(E)|^2 + D(E) |u_k(E)|^2 \right)}{|q'(E)|^2 \cosh^2 |q'(E)| L + k_F^2 \sinh^2 |q'(E)| L} \quad (4.25)$$

where

$$C(E) = \frac{4k_F^2 |u_k(E)|^2 q^2(E) \left[\left(|q'(E)|^2 + k_F^2 \right)^2 \sinh^2 |q'(E)| L + 4k_F^2 |q'(E)|^2 \right]}{N_2(E) + N_3(E)} \quad (4.26)$$

$$D(E) = \frac{4k_F^2 |v_k(E)|^2 q(E)^2 \left[\left(|q'|^2 + k_F^2 \right)^2 \sinh^2 |q'(E)| L \right]}{N_2(E) + N_3(E)} \quad (4.27)$$

while $N_1(E)$, $N_2(E)$ and $N_3(E)$ are defined as

$$N_1(E) = \left(\frac{q(E)^2}{q(E)^2 \cos^2 q(E) L + k_F^2 \sin^2 q(E) L} \right) \quad (4.28)$$

$$N_2(E) = |u_k(E)|^4 \left[\left(q(E)^2 + k_F^2 \right)^2 \sin^2 q(E) L + 4k_F^2 q(E)^2 \right] \times \left[\left(|q'(E)|^2 + k_F^2 \right)^2 \sinh^2 |q'(E)| L + 4k_F^2 |q'(E)|^2 \right] \quad (4.29)$$

$$N_3(E) = |v_k(E)|^4 \left[\left(q(E)^2 - k_F^2 \right)^2 \sin^2 q(E) L \right] \times \left[\left(|q'(E)|^2 + k_F^2 \right)^2 \sinh^2 |q'(E)| L \right] \quad (4.30)$$

Where $q(E)$ and $q'(E)$ are $q(E) = \sqrt{\frac{2m}{\hbar^2}(E - U)}$ and $q'(E) = i\sqrt{\frac{2m}{\hbar^2}(E + U)}$.

As shown in Fig. 4.2, for large U and thick L ($Lk_F > 1$), the shapes of both current density and conductance spectra are similar to those in the Delta-function model in the case where Z is large. One can obtain the results similar to those in the Delta-function model when Z is small by, taking L to be thin (see Fig. 4.2 in the case where $Lk_F = 0.5$ and Fig. 4.3 where $Lk_F = 2$).

In the Finite-width model, one can obtain oscillation features in the current density and conductance spectra, which cannot be reproduced by the Delta-function model, when U is small and L is thick enough (see Fig. 4.4 and Fig. 4.5 for $Lk_F = 50$). Similar to the oscillations occurring in MIM junctions in the Finite-width model, the oscillations in MIS tunneling spectra occur due to the properties of the insulating layer. The distance in energy between peak to peak in the conductance spectrum is

$$\Delta E_n = \frac{\hbar^2}{2m}\left(\frac{\pi}{L}\right)^2 (2n+1) \quad (4.31)$$

where n is positive integer (n = 1, 2, 3…) and L is the thickness of the insulator. Note that the first peak occurs at the energy which is must be greater than both Δ and U.

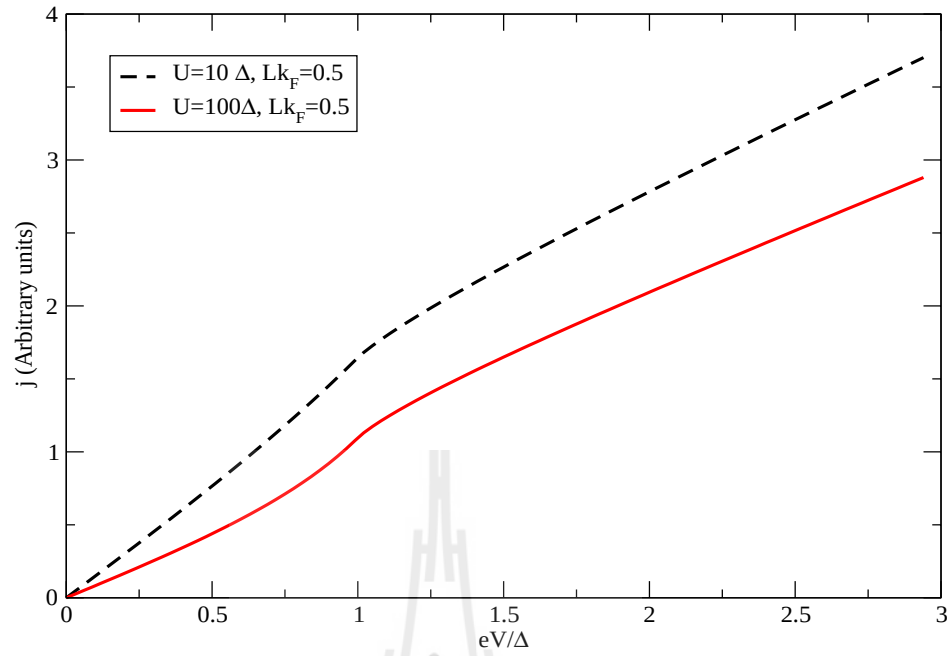

Figure 4.2 The plots of (a) current density j and (b) conductance G as a function of applied voltage at different the barrier potential U = 10 Δ and 100 Δ, when the thickness Lk_F = 0.5. Δ = 0.01 E_F.

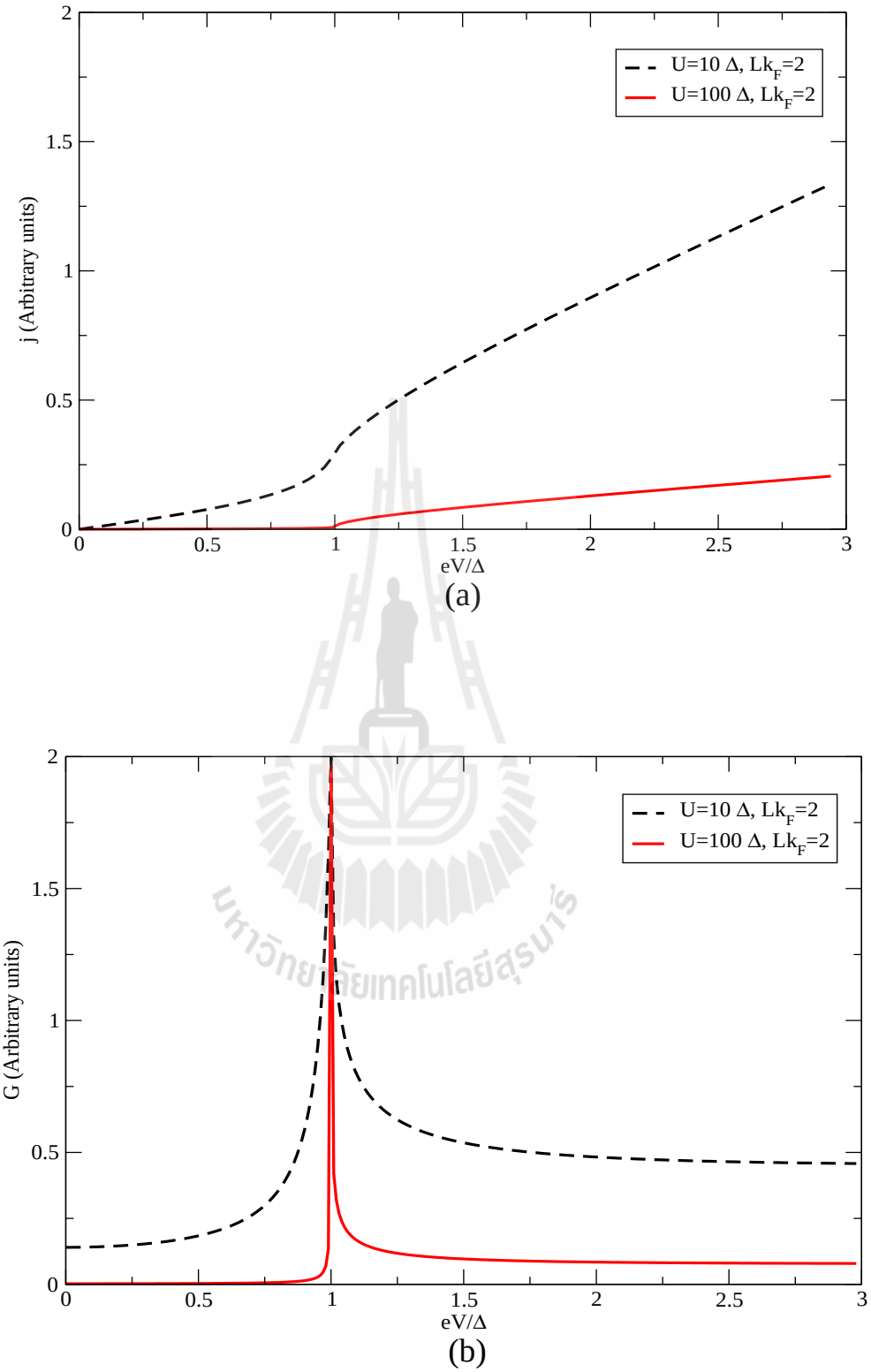

Figure 4.3 The plots of (a) current density j and (b) conductance G as a function of applied voltage at different the barrier potential U = 10 Δ and 100 Δ, when the thickness Lk_F = 2. Δ = 0.01 E_F.

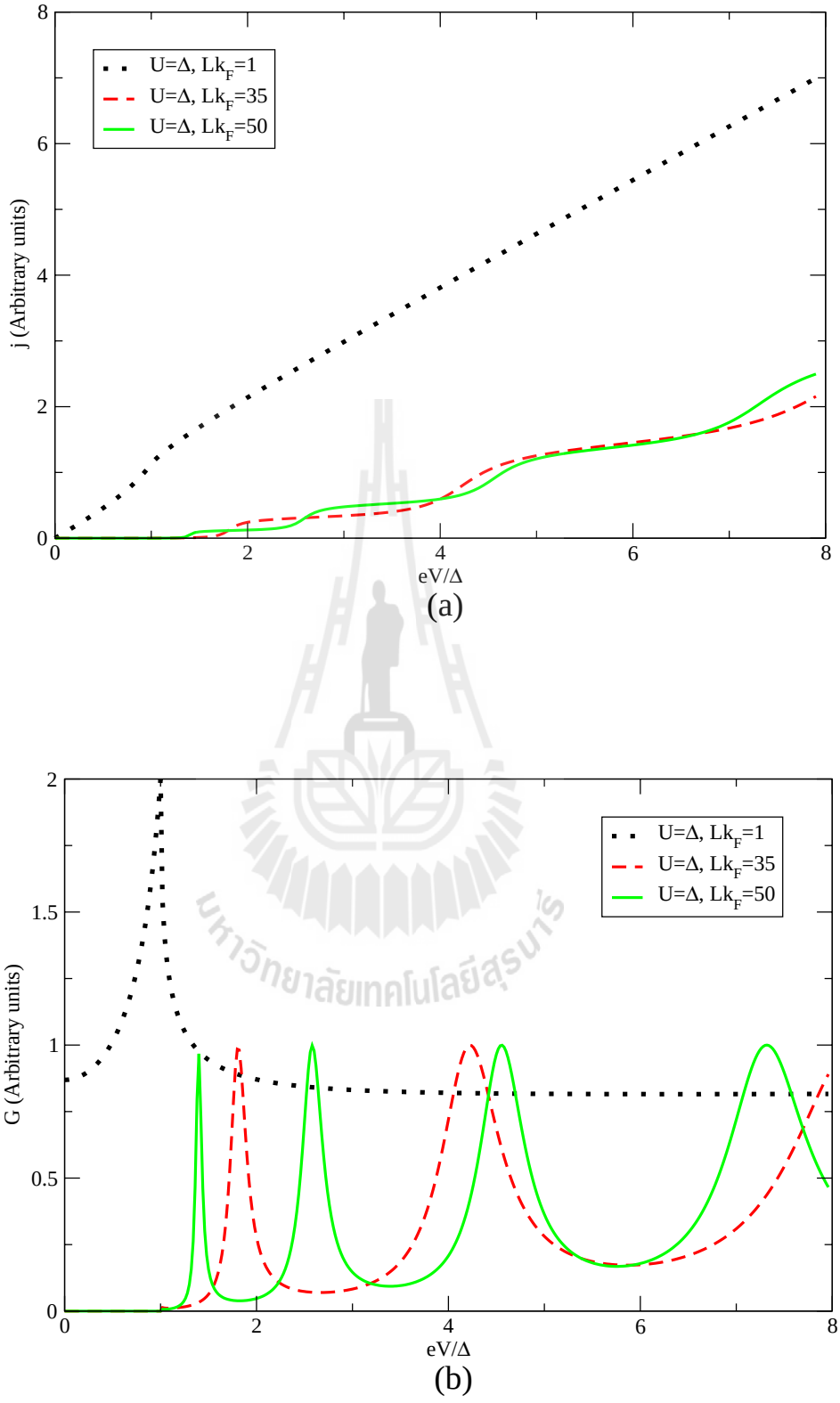

Figure 4.4 The plots of (a) current density j and (b) conductance G as a function of applied voltage at different the thickness Lk_F = 1, 35 and 50, when the potential barrier $U = \Delta$. $\Delta = 0.01\ E_F$.

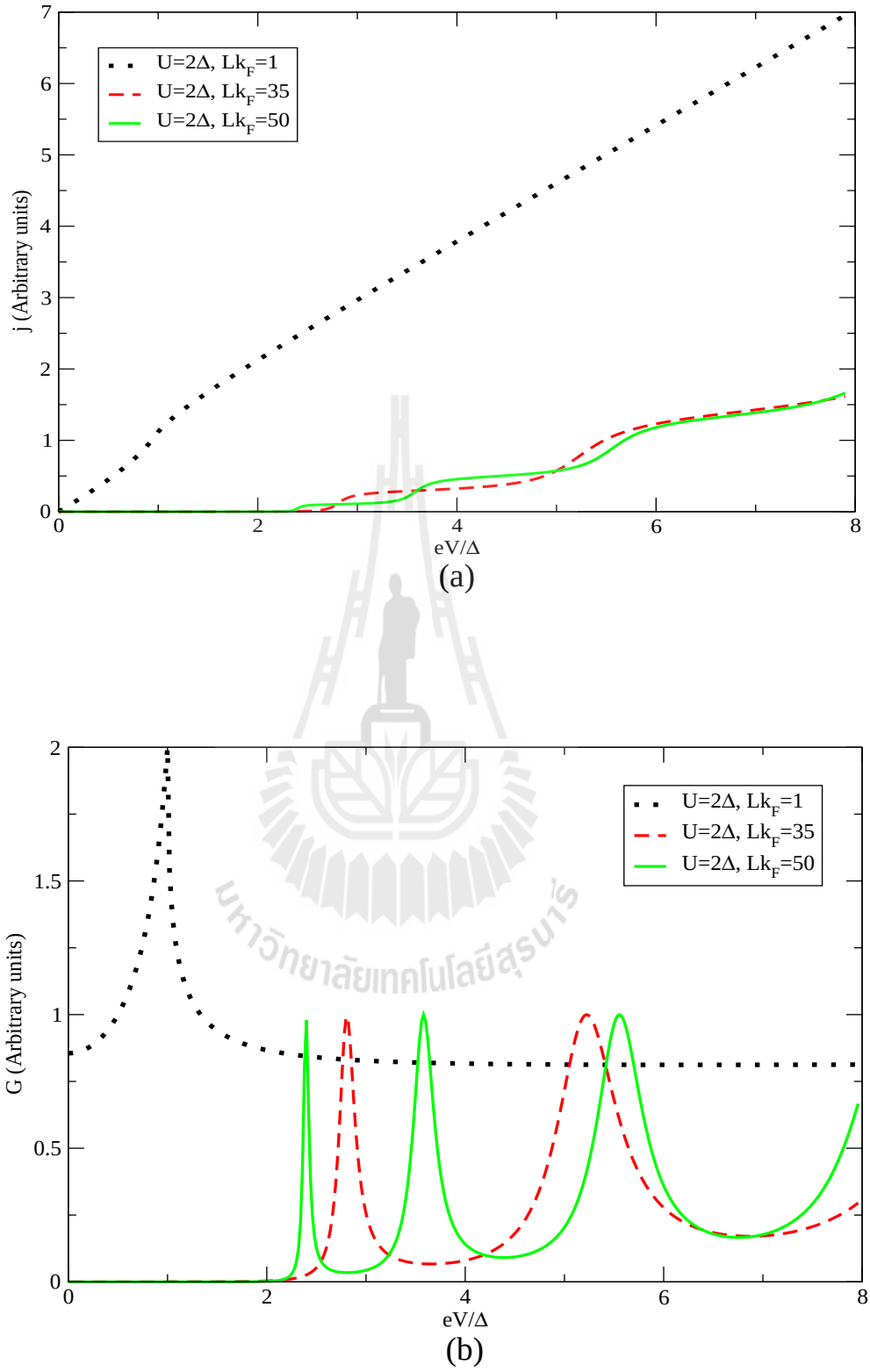

Figure 4.5 The plots of (a) current density j and (b) conductance G as a function of applied voltage at different the thickness Lk_F = 1, 35 and 50, when the potential barrier $U = 2\,\Delta$. $\Delta = 0.01\ E_F$.

The peak-to-peak distance is increased with *n*. When the insulating layer is thicker, the peak-to-peak distance in the conductance spectrum is shorter.

4.3 Comparison and Equivalency of the Two Models

Similar to MIM junction, one can see that the Finite-width model is more realistic in representing the real systems. It provides more information about the insulating layer than the Delta-function model, i.e., one can see oscillations occurring in both current density and conductance spectra at the voltage higher than the barrier potential. This feature cannot be seen if one uses the Delta-function model to represent the junction.

The current density and conductance spectra in the Finite-width model are similar to those in the Delta-function model, when the applied voltage is less than the barrier potential and in the limit where the thickness L of the insulator region is small. This similarity suggests that one can find the equivalency of the two models when the insulating layer of the junction is thin. To obtain the equivalency, like in the case of MIM junction, one can compare the value of the conductance at zero voltage from the two models. The conductance at zero voltage from the Delta-function model is

$$G_D(eV=0,Z)=\frac{2}{(2Z^2+1)^2} \tag{4.32}$$

and the conductance at zero voltage from the Finite-width model is

$$G_F\left(eV=0,L,U\right)=\frac{2}{\left(\left(\frac{\left(U+E_F\right)^2}{4UE_F}\right)\cosh\left(\left(2\sqrt{\frac{U}{E_F}}\right)Lk_F\right)-\left(\frac{\left(U-E_F\right)^2}{4UE_F}\right)\right)^2} \tag{4.33}$$

where k_F and E_F are the Fermi wave vector and the Fermi energy of the superconductor region. By considering in the limit of $\left(2\sqrt{U/E_F}\right)Lk_F << 1$ and comparing the two equations above and, one can obtain the relation of the parameter Z from the Delta-function model and the parameters U and L from the Finite-width model as

$$Z = \frac{\left(U + E_F\right)}{2E_F} Lk_F \tag{4.34}$$

which is the exactly the same as that for MIM junction. This result is not very surprising because it is the properties of the insulating layer being considered, independent of the properties the materials on either side of the layer.

The relation in Eq. (4.34) can provide the same shapes of current density and conductance spectra from the two models within 10% as long as

$$Lk_F \leq \sqrt{\frac{2E_F^{3/2}}{3\sqrt{U}(U + E_F)}} \tag{4.35}$$

which is again the same as in the case of MIM junction

In Figs. 4.6 and 4.7, the plots of the current density and conductance spectra from the two models using the insulating parameters according to Eq. (4.34) and the condition (4.35) are shown.

As shown in Figs. 4.6 and 4.7, both current density and conductance spectra from the two models are the same within 10%. The results get worse as the thickness L gets larger or the potential gets bigger. Again, it is worth noted that the bigger values of L affect the similarities of the two models more than the higher barrier potential.

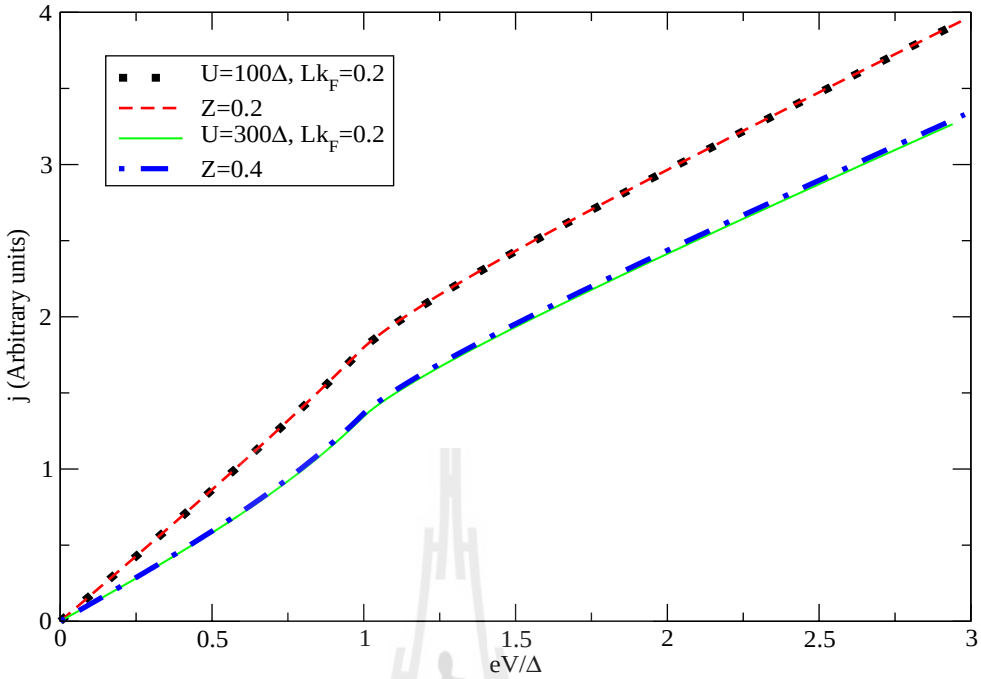

(a)

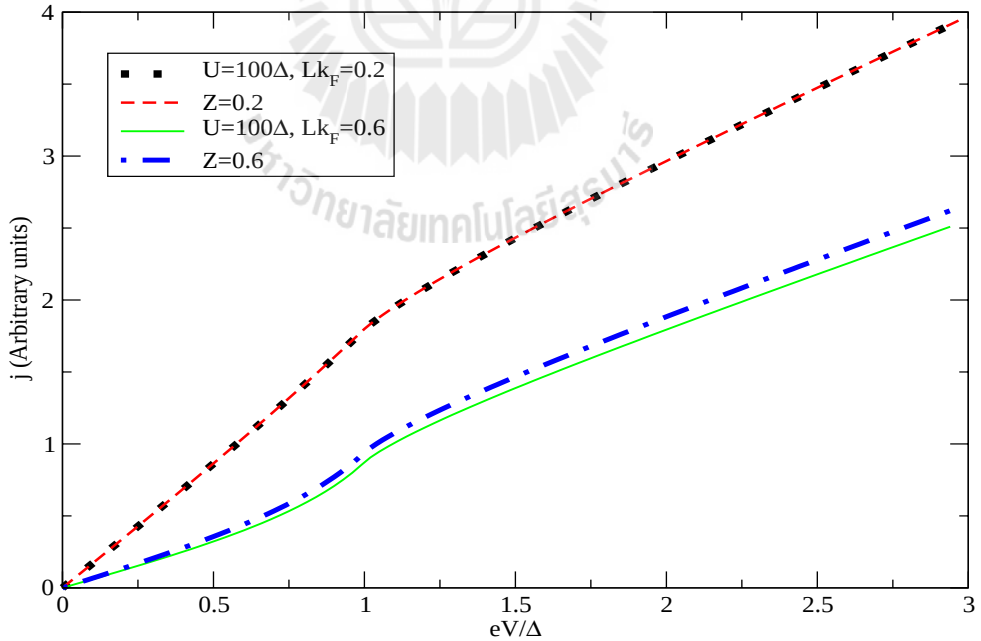

(b)

Figure 4.6 The plot of current density spectra with (a) thickness Lk_F = 0.2 (for U = 100 Δ, Z = 0.2 and for U = 300 Δ, Z = 0.4) and (b) the barrier potential U = 100 Δ (for Lk_F = 0.2, Z = 0.2 and for Lk_F = 0.6, Z = 0.6). Δ = 0.01 E_F.

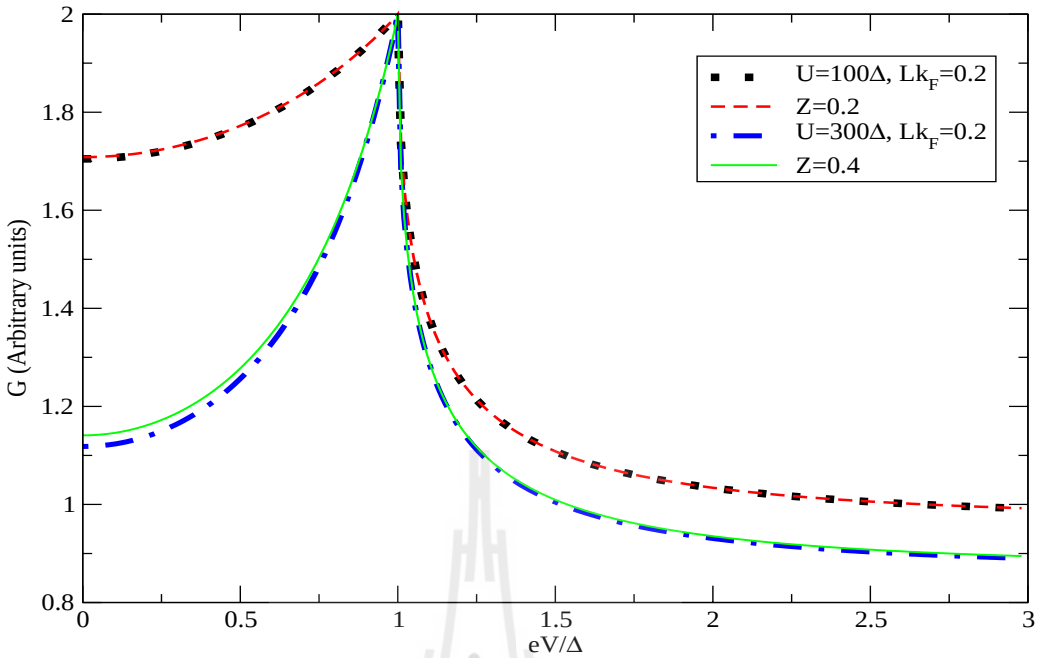

(a)

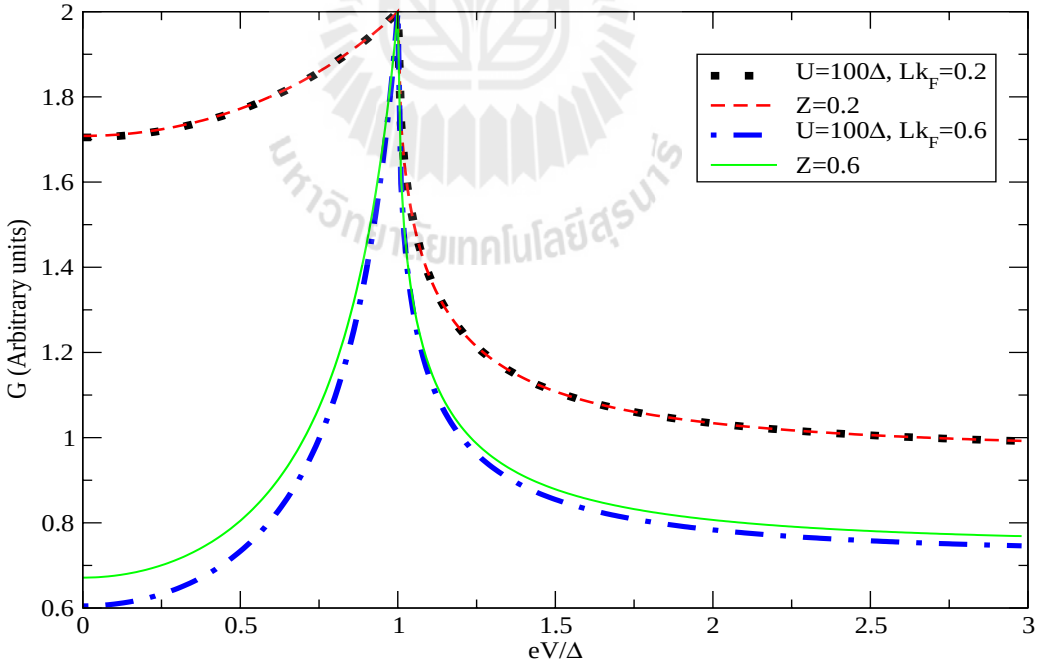

(b)

Figure 4.7 The plot of conductance spectra with (a) thickness Lk_F = 0.2 (for U = 100 Δ, Z = 0.2 and for U = 300 Δ, Z = 0.4) and (b) the barrier potential U = 100 Δ (for Lk_F = 0.2, Z = 0.2 and for Lk_F = 0.6, Z = 0.6). Δ = 0.01 E_F.

4.4 Conclusions

In this chapter, the tunneling current density and conductance spectra of MIS junction in both Delta-function and Finite-width models are examined. In the Delta-function model, the spectra depend strongly on the barrier strength *Z*, and in the Finite-width model, they depend on *U* and *L*. The shapes of both current density and conductance spectra from the Finite-width model are similar to those from the Delta-function model when the applied voltage is less than *U*. More specifically, when *L* is thin, the shapes are similar to those in the Delta-function model when *Z* is small and, when *L* is thick they are similar to those in the Delta-function model when *Z* is big.

The Delta-function model cannot produce oscillations in the current density and conductance spectra. These oscillations are seen in the Finite-width model when the applied voltage is higher than the barrier potential. The peak-to-peak distance of the oscillation is not constant and depends on the thickness of the barrier. One learns from these results that as long as the main features, in which one is interested, do not occur at higher energy scale than the barrier potential (which is always the case for MIS junction) and the insulating layer is made thin enough, the Delta-function model can be used to study MIS junction and the parameter *Z* can be related to *U* and *L* according to Eq. (4.34).

CHAPTER V

CONCLUSIONS

In the thesis, the current density and conductance spectra of the both one-dimensional MIM and MIS junctions in two models are investigated by using the scattering method. In the Delta-function model, the insulator is represented by a delta-function barrier potential, which is characterized by a unitless parameter *Z*. In the Finite-width model, the insulator is represented by a layer of thickness *L* with a barrier potential *U*. Eventhough, the latter model is obviously more realistic, it is much more complicated because it involves more parameters and more interfaces. Therefore, one would incline to use the Delta-function model because of its simplicity. One of the questions, which this work is done to find the answer for, is when it is reasonable to use the Delta-function model in place of the Finite-width model.

It is found in this work that both limitations in and the conditions for using the Delta-function model is independent of the types of junctions, i.e., they are the same for both MIM and MIS junctions, since they are related to the properties of the insulator. Both Delta-function and Finite-width models give *similar* results for both types of junctions as long as the applied voltage is less than the barrier potential. This is usually the case because the barrier potential in most experiments are of order *eV* or more, while the range of interest of the applied voltage is of order *meV* or less.

It is shown in this thesis that the Delta-function model can only be used in

place of the Finite-width model only when $Lk_F << \frac{1}{2}\sqrt{\frac{E_F}{U}}$, where k_F and E_F are the Fermi wave vector and energy of the metal respectively. (Note that U is generally is of the same or one order of magnitude smaller than E_F.) When this condition is satisfied the two models can be used interchangeably and the parameters characterizing the insulator from both models are related to one another through the following expression.

$$Z = \frac{(U + E_F)}{2E_F} Lk_F \tag{5.1}$$

More specifically, if

$$Lk_F \leq \sqrt{\frac{2E_F^{3/2}}{3\sqrt{U}(U + E_F)}} \tag{5.2}$$

The current density and conductance spectra of both MIM and MIS junctions obtained from both models are the same within 10%, if one uses the relation (5.1) within the condition (5.2) is satisfied.

When the applied voltage is higher than the barrier potential, the current density and conductance spectra obtained from the Finite-width model contain oscillations. These oscillations cannot be explained by the Delta-function model. The first peak of the oscillation occurs at the applied voltage just higher than U. The distance in energy between two adjacent peaks is not constant, as can be seen from the following relation.

$$\Delta E_n = \frac{\mathrm{h}^2}{2m}\left(\frac{\pi}{L}\right)^2 (2n+1) \tag{5.3}$$

where n is a positive integer. This finding indicates that if one needs to obtain the information about the insulator from tunneling spectroscopy, one will need to apply

high voltage and use the Finite-width model to represent the system.

REFERENCES

REFERENCES

Andreev, A. F. (1964). The thermal conductivity of the intermediate state in superconductors. **Sov. Phys. JEPT.** 19: 1228.

Bardeen, J., Cooper, L. N., and Schrieffer, J. R. (1957). Theory of superconductivity. **Phys. Rev.** 108 (5): 1175-1204.

Blonder, G. E., Tinkham, M., and Klapwijk, T. M. (1982). Transition from metallic to tunneling regimes in superconducting microconstrictions: Excess current, charge imbalance and supercurrent conversion. **Phys. Rev. B** 25 (7): 4515-4532.

Blonder, G. E. and Tinkham, M. (1983). Metallic to tunneling transition in Cu-Nb point contacts. **Phys. Rev. B** 27 (1): 112-118.

Griffin, A. and Demers, J. (1971). Tunneling in the normal-metal-insulator-superconductor geometry using the Bogoliubov equations of motion. **Phys. Rev. B** 4 (7): 2202-2208.

Giaever, I. (1960). Energy gap in superconductors measured by electron tunneling. **Phys. Rev. Lett.** 5 (4): 147-148.

Lykken, G. I., Geiger, A. L., and Mitchell, E. N. (1970). Measurement of the Fermi velocity in single-crystal films of lead by electron tunneling. **Phys. Rev. Lett.** 25 (22): 1578-1580.

Lykken, G. I., Geiger, A. L., Dy, K. S., and Mitchell, E. N. (1971). Measurement of the superconducting energy gap and Fermi velocity in single-crystal lead films by electron tunneling. **Phys. Rev. B** 4 (5): 1523-1529.

McMillan, W. L. and Anderson, P. W. (1966). Theory of geometrical resonances in the tunneling characteristics of thick films of superconductors. **Phys. Rev. Lett.** 16 (3): 85-87.

Nesher, O. and Koren, G. (1999). Observation of Tomasch oscillations and tunneling-like behavior in oxygen-deficient edge junctions. **Phys. Rev. Lett.** 74 (22): 3392-3394.

Nesher, O. and Koren, G. (1999). Measurements of Δ and v_F from Andreev reflections and McMillan-Rowell oscillations in edge junctions of $YBa_2Cu_3O_{6.6}/YBa_2Cu_{2.55}O_y/YBa_2Cu_3O_{6.6}$. **Phys. Rev. B** 60 (13): 9287-9290.

Nicol, J., Shapiro, S., and Smith, P. H. (1960). Direct measurement of the superconducting energy gap. **Phys. Rev. Lett.** 5 (10): 461-464.

Rowell, J. M. and McMillan, W. L. (1966). Electron interference in a normal metal induced by superconducting contacts. **Phys. Rev. Lett.** 16 (11): 453-456.

Shkedy, L., Aronov, P., Koren, G., and Polturak, E. (2004). Observation of McMillan-Rowell like oscillations in underdoped $YBa_2Cu_3O_y$ junctions oriented along the node of the d-wave order parameter. **Phys. Rev. B** 69: 132507-1-132507-4.

Tinkham, M. (1996). **Introduction to superconductivity** (2^{nd} ed). USA: McGraw-Hill, Inc.

Tomasch, W. J. (1965). Geometrical resonance in the tunneling characteristics of superconducting Pb. **Phys. Rev. Lett.** 15 (16): 672-675.

Tomasch, W. J. (1966). Geometrical resonance and boundary effects in tunneling from superconducting In. **Phys. Rev. Lett.** 16 (1): 16-19.

Tsokur, E. B., Yarygin, A. V., Yusupov, K. T., Aminov, B. A., Hein, M. A., Muller, G., Piel, H., Wehler, D., Kresin, V. Z., Rosner, D., Winzer, K., and Wolf, Th. (1995). Manifestation of a clear gap structure from point-contact and tunneling spectroscopy of $YBa_2Cu_3O_{7-x}$ and $YBa_2Cu_3O_{7-x}$ single crystals. **Phys. Rev. B** 52 (2): 1352-1357.

Wolf, E. L. (1989). **Principle of Electron Tunneling Spectroscopy**. USA: Oxford University Press, Inc.

CURRICULUM VITAE

Mr. Rarm Phinjaroenphan

Date of birth: 29 July 1981

Place of birth: Nakhon Ratchasima, Thailand.

Nationality: Thai

Education

Academic year	
1999-2002	Kasetsart University, Bangkok, Thailand.
	Bachelor of Science (Physics)
2004-2006	Currently enrolling in Master degree majoring in Physics
	Science, Suranaree University of Technology, Nakhon
	Ratchasima, Thailand.